Available online at www.CivileJournal.org

Civil Engineering Journal

(E-ISSN: 2476-3055; ISSN: 2676-6957)

Vol. 8, No. 05, May, 2022

Investigation of Honeycomb Sandwich Panel Structure using Aluminum Alloy (*AL6XN*) Material under Blast Loading

Dany Taufiq Alim Ansori [1], Aditya Rio Prabowo [1*], Teguh Muttaqie [2], Nurul Muhayat [1*], Fajar Budi Laksono [3], D. D. Dwi Pria Tjahjana [1], Ari Prasetyo [4], Yemi Kuswardi [5]

[1] *Department of Mechanical Engineering, Universitas Sebelas Maret, Surakarta 57126, Indonesia.*

[2] *Research Center for Hydrodynamics Technology, National Research and Innovation Agency (BRIN), Surabaya 60112, Indonesia.*

[3] *Department of Research and Development, P.T. DTECH Inovasi Indonesia, Salatiga 50742, Indonesia.*

[4] *Department of Mechanical Engineering, Vocational School, Universitas Sebelas Maret, Surakarta 57126, Indonesia.*

[5] *Department of Mathematics Education, Universitas Sebelas Maret, Surakarta 57126, Indonesia.*

Received 19 February 2022; Revised 18 April 2022; Accepted 25 April 2022; Published 01 May 2022

Abstract

In this study, we focused on the large inelastic behavior of a sandwich panel made of two solid plates as a stiffener and a honeycomb core shell subjected to blast load. The loading scheme was carried out using an explosive charge bullet mounted at a standoff distance of 100 mm with three mass variations of trinitrotoluene: 1, 2, and 3 kg TNT. The numerical simulations performed using ABAQUS/CAE were validated with the experimental results of a previous study. The geometrical effects of the sandwich panel on intact and damaged models were also numerically investigated. The panel was designed using a square and hexagonal honeycomb core. The effect of honeycomb core height was also observed by modeling the core using three height variations: 31, 51, and 71 mm. The results showed that the hexagonal core was more resistant to blast loads than the square design. The core height parameter determines the energy absorption based on these results. The structural strength is also affected by the damage. The findings of this study can be used to improve structural designs that utilize sandwich panels to withstand blast loads.

Keywords: Blast Loads; Deformation; Honeycomb; Trinitrotoluene; ABAQUS/CAE.

1. Introduction

Ship construction is a combination of art and science, the result of the hard work of engineers. The rapid development of technology requires designers and engineers to be innovative to make new discoveries and have positive impacts on human life. In the shipping industry, there have been many breakthroughs, especially in terms of the material technology and construction systems used on ships. Steel plate is one component that plays an important role in the manufacture of ship structures, especially in the hull. The hull structure must have high strength to withstand explosive forces or loads when something unexpected happens. Especially on ships serving in combat operations, the structure of the ship is very prone to damage. Warships can experience air explosions, which, if occurring near the ship, can damage the ship's wall structure and cause the ship to suffer complete damage [1]. This has prompted engineers around the world to try to develop design and analytical methods to protect against structural failure due to blast loads [2].

* Corresponding author: aditya@ft.uns.ac.id; nurulmuhayat@staff.uns.ac.id

http://dx.doi.org/10.28991/CEJ-2022-08-05-014

Technological developments have given rise to software and computer programs that can be used to accurately model the behavior of materials or structural components. In this simulation, we used the ABAQUS/CAE Finite Element Method (FEM) package to model square and hexagonal sandwich panels using the finite element method. Studies have been carried out using the sandwich panel concept to reduce the damage caused by explosions. A sandwich panel is a composite structure between two steel plates as stiffeners separated by a core. This core can be a composite material or metal [3]. The sandwich structure acts as an energy absorber from the explosion in this structural arrangement. These panels will propagate the mechanical impulses transmitted into the design as well as reduce the stresses exerted on the protected structure behind the panels.

This work builds on several previous studies that have examined ways to optimize energy absorption capacity and maintain deflection in panels. Dharmasena et al. carried out experimental tests to study the dynamic mechanical response of a square honeycomb core sandwich panel to blast loads [4]. The use of square cores in this study is also supported by previous research by Xue and Hutchinson, who studied the effectiveness of square honeycomb sandwich cores in absorbing blast waves simulated using software. The study agreed that square honeycomb cores are effective for sandwich plates in all metals because they combine excellent crushing strength and energy absorption [5]. This study did not discuss the effect of the core shape of the sandwich panel on its response to blast loading. This was refined by Yu et al., Ma et al., and Liu et al., who used several types of honeycomb cores, including Y-shaped cores, kirigami-inspired pyramid foldcores, and U-type corrugated cores with various types of loading [6–8]. Sandwich panel cores were also investigated by Zhu and Lu, who studied the structural response of sandwich panels from blast loads, especially for pyramidal cores, diamond-celled cores, corrugated cores, hexagonal honeycomb cores, and square honeycomb cores [9]. The results prove that the selection of the honeycomb core has an influence on the strength of the sandwich panel structure. In addition to the selection of core geometry, the material used also determines the strength of the sandwich structure. Cerik used aluminum alloy plates to obtain its response to blast loads [10]. Research on the use of these materials is also supported by Li et al., who used aluminum foam-cored sandwich panels to be tested against blast loads. The results show that the structural ductility of aluminum alloys is influential when rectangular plates and rigid panels are subjected to sudden lateral stresses [11]. Deqiang et al. added to the literature by using adhesively bonded aluminum sandwich panels to examine surface and honeycomb core damage [12].

Several studies have shown that the configuration of the sandwich panel structure still needs to be realized to optimize its function in resisting air blast loads. Nayak et al. presented a sandwich panel optimization method against the effects of air blast loading by increasing the thickness of the front plate, which can distribute the load to a wider core area [13]. However, variations in height and its effect on sandwich plate strength have not been discussed in several of the studies above. In this study, a simulation was carried out to compare the deflections in several sandwich panel configurations. We compare the shape of the honeycomb square and hexagonal core made with three different core heights, 31, 51, and 71 mm. The model was developed to determine the effect of geometry and core height on the strength of the sandwich panels. The sandwich panel structure was made using stainless steel alloy (AL6XN). Previous studies also never observed the response of a deformed sandwich panel structure to whether it is still effective to withstand a given load. The damaged model is also modeled in this study to compare with the intact structure on how the deformed structure responds to the deflection of the sandwich panel structure.

2. Fundamentals of Blast Loading

2.1. Explicit Dynamic Analysis

Explicit dynamic simulation analysis refers to the application of explicit integration rules along with the use of the mass matrix of diagonal ("lumped") elements. The equations of motion for the body are integrated using the explicit integration rules shown in Equation 1.

$$\dot{u}^N_{(i+\frac{1}{2})} = \dot{u}^N_{(i+\frac{1}{2})} + \frac{\Delta t_{(i+1)}+\Delta t_{(i)}}{2}\ddot{u}^N_{(i)}, \quad (1)$$

$$\dot{u}^N_{(i+1)} = \dot{u}^N_{(1)} + \Delta t_{(i+1)}\dot{u}^N_{(i+\frac{1}{2})}. \quad (2)$$

where $\dot{u}^N$ represents the degrees of freedom and the subscript i is the number of increments in the explicit dynamics step; the center difference integration operator explicitly uses the known values of $\dot{u}^N_{(i+\frac{1}{2})}$ and $\ddot{u}^N_{(i)}$ from the previous increment.

The explicit integration rule is fairly simple, but the explicit dynamics procedure does not provide adequate computational efficiency. The use of the mass matrix of the diagonal elements can be used as a computational efficiency solution of the explicit procedure because the acceleration at the start of the increment is calculated by:

$$\ddot{u}^N_{(i)} = (M^{NJ})^{-1}\left(P^J_{(i)} - I^J_{(i)}\right). \quad (3)$$

where M^{NJ} is the mass matrix, P^J is the applied load vector, and I^J is the internal force vector. The combined mass matrix is used because the inverse is simple to calculate and because the vector product of the reciprocal of mass by the inertial force requires only n operations, where n is the number of degrees of freedom in the model. For details on the explicit dynamic's procedure, see the ABAQUS Explicit User's Manual.

2.2. Air Blast Overpressure

The explosion releases a large amount of potential energy into the surrounding air in the form of heat and shock waves. Shock waves can be categorized into two types—detonation and deflagration—depending on their intensity and speed. Detonation is a shock wave that propagates at high speed due to high-pressure gas spreading away from the center of the explosion and then compressing the surrounding air. Deflagration is a shock wave. Low dispersion at subsonic velocities is associated with slow heat and mass transfer phenomena [14]. Air Blast Overpressure (ABO) is a phenomenon of increasing air pressure in a short time to be above atmospheric pressure. ABO occurs due to a chemical explosion. The detonation equilibrium parameters are determined by the detonation speed, pressure, and explosion temperature [12]. Currently, explosion phenomena can be simulated using theoretical and numerical approaches. The two most popular approaches to calculating Air Blast Overpressure (ABO) are the CONWEP air blast and the CEL models. However, an explosion simulation will be carried out using the CONWEP model in this simulation.

In this simulation based on an experiment, the shock wave propagates at supersonic speed, which can be idealized as a detonation. Condensed high explosives produce gases with high temperatures and pressures of up to 300 kbar. This hot gas then expands and leaves the volume it occupies.

The blast wave creates a pressure value well above the ambient atmospheric pressure, which is referred to as side-on overpressure. This pressure decays as the shock wave moves away from the center of the explosion and will then drop below ambient pressure quickly and create a negative phase. Figure 1 shows a typical blast pressure profile.

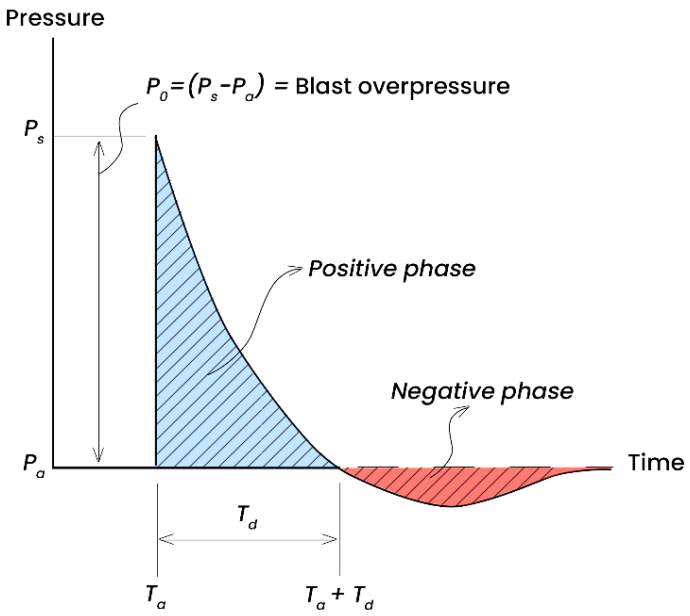

Figure 1. The typical blast pressure profile

After the arrival time of the explosion ta, there is an increase in pressure in a very short time until it reaches the peak value of overpressure ps, above the pressure around pa. Then, there will be a sudden decrease in the pressure value to the ambient level after the duration of td, then decay further down negative pressure (creating a partial vacuum/negative phase). A modified Friedlander equation (Equation 4) can describe the pressure response with time.

$$p(t) = (p_s - p_a)\left[1 - \frac{t-t_a}{t_d}\right] e^{-(t-t_a)/\theta}. \quad (4)$$

where p_a is the ambient pressure, t is overall duration, t_a is the arrival time, t_d is the positive phase's duration, and θ is the time decay constant [8]. The peak pressure of the blast wave (P) can be written using Equation 5.

$$P = K\left[\frac{m}{r^3}\right] \quad (5)$$

where K is an explosive material parameter, m is the explosive mass, and r is the standoff distance [4].

2.3. CONWEP Charge for Incident Waves Structure

The blast wave parameters such as pressure and peak impulse, duration of positive or negative phase, and time of arrival are defined as a function of the scale distance and weight of the explosive charge. According to Hopkinson-Cranz, the scaling law can be used to correlate the effects of proximity to the center explosion and the weight of the explosive charge on the generation of shock waves. The law of the distance scale (Z) is defined as:

$$Z = \frac{R}{W^{\frac{1}{3}}}. \tag{6}$$

where R is the stand-off distance, which is the distance from the center of the blast to the target surface. The further the center of the explosion from the surface, the less structural damage caused by the blast wave. W is the weight of the explosive charge.

The total air blast overpressure (P_{total}) is obtained by combining the incident angle (θ) depending on the incident overpressure (P_{io}) and reflected overpressure (P_{ro}) [14]. The total air blast overpressure is defined as:

$$P_{total} = \begin{cases} [P_{ro}(t) - 2P_{io}(t)cos\theta^2 + [cos\theta + 1]P_{io}(t), cos\theta \geq 0], \\ P_{io}(t), cos\theta < 0 \end{cases} \tag{7}$$

$$P_{io}(t) = (P_{so} - P_a)\left(1 - \frac{t - t_a}{t_0}\right)e^{-\left(\beta\frac{t-t_a}{t_0}\right)}, \tag{8}$$

$$P_{ro}(t) = 2P_{io}(t) + \frac{(\gamma+1)\{P_{io}(t)\}^2}{2\gamma P_a + (\gamma-1)P(t)}. \tag{9}$$

where P_{so} represents the peak incident pressure, P_a denotes ambient pressure, t_a represents the arrival time of the blast wave propagating to the target surface, t_0 is the time duration of the positive phase, β is a dimensionless decay coefficient that depends on the shape of the shock wavefront [15], and γ is the ratio of the specific heat of air [14].

The pressure is applied to the front surface of the sandwich panel and defined using a spatially distributed function for explosive materials. The weight of the explosion and the distance to the blast's center are determined to perform this test. CONWEP is a well-known air blast loading program developed by the U.S. Army Research and Development Center for Engineers (ERDC) [14]. This program is an empirically determined air blast model. This test model is based on various explosion tests that have been carried out by Dharmasena et al. [4]. The authors performed this computation on the Asus S406UA-BM165T computer of 1.6 GHz, RAM 8GB, Windows 10 Home, Intel HD Graphics.

2.4. Air Blast Experiment

The experiment was carried out in previous studies using a test panel. The test scheme was a cylindrical explosive charge bullet mounted on an axis parallel to the center of the sandwich panel and placed at a standoff distance of 100 mm from the surface of the sandwich panel. Experiments were carried out with three variations of explosive mass using TNT 1, 2, and 3 kg. Figure 2 shows the schematic of the explosion test on a sandwich panel structure. This image is modified from the experimental work carried out by Dharmasena et al. [4].

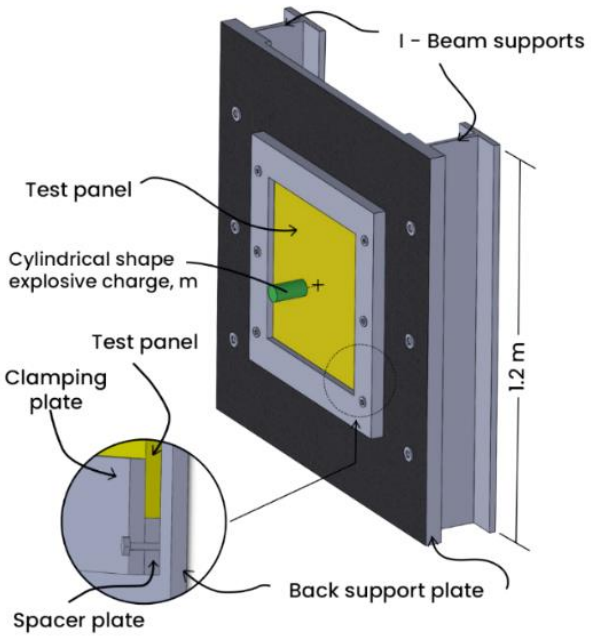

Figure 2. Explosion loading scheme re-drawing based on reference [4]

The shock wave propagates from the source of the explosion to the front face of the sandwich panel before it is reflected. The pressure generated from the shock wave decays with distance and time. When a shock occurs on a rigid surface, the shock wave will be reflected. A larger pressure reflection coefficient occurs when the gas effect is real (dissociation and ionization of air molecules). Deshpande and Fleck refer to the initial phase of this explosion shock structure interaction as Phase I [16]. Figure 3 shows how the explosion process in a sandwich panel structure, starting from applying an impulse to the front face of the structure (Figure 3-a), causes it to gain velocity (Figure 3-b).

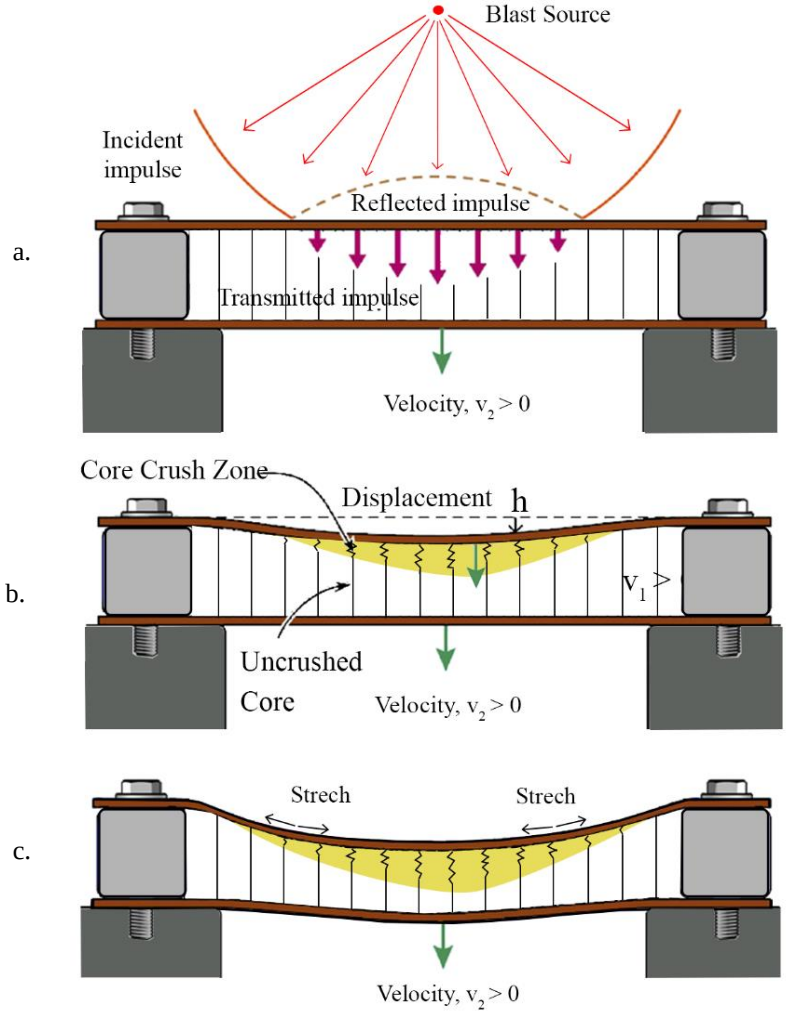

Figure 3. Dimension of sandwich panel structure re-drawing based on reference [4]

The core crushing begins when the front plate is subjected to stress due to the applied impulse. The core serves to restrain and slow down the movement of the front plate (stage II) [16]. For weak explosive shocks, it is possible to resist core densification at the front face. The strength of this crushing depends on the relative core density, the topology of the cell, and material properties.

The impulses transmitted to the back face sheet can cause the edge supported panel to bend for large blast loads, as shown in Figure 3c. In stage III, damaged honeycomb core plays a significant role, as the highly impact resistant core can generate a shearing force that accompanies plastic dissipation sufficient to resist panel movement before the load applied to the supporting structure exceeds the design strength, and tears occur on the front face [4].

2.5. Typical Damages in Sandwich Structure

Since the face sheet is a thin structure and the core is relatively weak, the sandwich panel structure is susceptible to damage when local loads, such as impact loading and indentation, are applied [17]. This study suggests that core damage plays an essential role in the fractured sandwich structure. When a local load is applied to the sandwich panel structure, the system is deformed. The front face, to which the load is applied, is deflected locally against the back face, followed by transverse deformation of the core material. When the load exceeds the elastic limit, the composite face sheet begins to deform and, subsequently, is followed by crushing the core around the loading point (Figure 4-a). When the gluing on the face sheet and core is not strong enough to withstand the load, debonding occurs between the face sheet and the core, causing permanent dents to occur in the core (Figure 4-b).

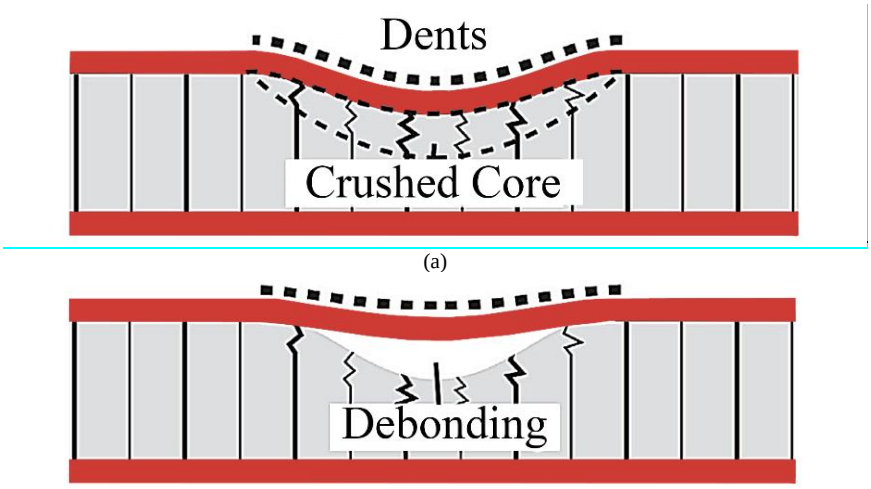

Figure 4. Schematic of impact damages in honeycomb sandwich structures re-drawing based on reference [17]

The sandwich structure has a high specific flexural stiffness because the core keeps the two face sheets apart. Due to the dent, the distance between the face sheets is reduced and causes stress concentration around the impacted area, resulting in unexpected failure.

2.6. State of The Art

FE simulation studies of sandwich structure models under blast loading have been carried out with various configurations. Cerik used an aluminum alloy plate to evaluate its response to explosive loads [10]. The results show that the ductility of the aluminum alloy material is influential when the plate is suddenly subjected to lateral stress. Sahoo et al. conducted explosion tests on monolithic and layered plates [18]. The results show that Mg has a smaller deflection compared to aluminum. Under ballistic impact, Yu et al. found that in the same acreage mass, a Y-shaped core sandwich structure has better impact resistance and energy absorption capacity than a laminated structure [6]. Liu et al. tested the U-type corrugated sandwich panel model under a quasi-static compression load and the results showed how the compression process occurred in the sandwich panel structure [19]. Research related to honeycomb core geometry was also carried out by Ma et al. and concluded that in average stress, pyramid sandwiches outperformed square honeycomb, eggbox, and Miura-Ori in compression, with improvements of 73%, 130%, and 342%, respectively [7]. The average shear stress value of the pyramid sandwich is 34% higher than that of Miura-Ori, but its value is 11% lower than square honeycomb.

Table 1. Previous research that underlies the study of sandwich panel structures under blast loads

Author	Phenomenon	Subject	Conclusion
Cerik (2017)	Explosion	Aluminum alloy-plated	The ductility of the aluminum alloy structure is very influential when rectangular plates and stiffened panels are subjected to sudden lateral stresses. HAZ also significantly affects plate permanent set [10].
Sahoo et al. (2017)	Explosion	Monolithic and layered plates	For monolithic plates of equivalent mass, deflection for Mg is less than half of that of Al and steel plates. For layered plates, the deflection is showing a decreasing trend with increasing layers of Al and SS [18].
Markose et al. (2017)	Blast loading	V-shaped plates	Inclined plates are generally more effective in reducing the applied impulse. Maximum reduction occurs at plates that have a minimum angle. Plates with lower angles of entry consistently provide lower deflection values when compared to flat plates. This occurs for various values of the charge mass [20].
Wowk et al. (2020)	Low-velocity impact	Honeycomb sandwich panel	Low-impact velocity resulted in the aluminum sandwich panel being damaged in the form of a dent on the front face and cell wall buckling just below the front face dent. The width of the damage that occurs in the honeycomb core is the same as the width of the dent on the front face [21].
Deqiang et al. (2020)	Surface and honeycomb core damage	Adhesively bonded aluminum sandwich panels	The presence of adhesive causes the folds that occur on the honeycomb core wall to be deeper. The depth of the cell wall folding of the honeycomb core increases with the height of the adhesive fillet height. [12].
Yu et al. (2021)	Ballistic impact	Y-shaped cores sandwich structure	The energy absorption ratio of the composite sandwich structure is greater than that of the laminate at the same collision speed. It has better impact resistance and energy absorption capacity than a laminated structure with the same acreage mass [6].

Ma et al. (2021)	Quasi-static compression load	Kirigami-inspired pyramid foldcore	Under average stress, the pyramid sandwich outperforms square honeycomb, eggbox, and Miura-Ori in compression, with increases of 73%, 130%, and 342%, respectively. The average shear stress value of the pyramid sandwich is 34% higher than that of the Miura-Ori, but its value is 11% lower than square honeycomb [7].
Zhao et al. (2021)	Blast loading	Steel–concrete–steel sandwich panel	The blast capacities of steel–concrete–steel (SCS) sandwich, concrete–steel–concrete (CSC), and reinforced concrete (RC) slabs were investigated. The thickness of the steel plate has a significant role in resisting the blast loads. Thus, the SCS slab has excellent blast resistance [22].
Jing et al. (2021)	Air blast loading	Square sandwich panels with layered-gradient foam cores (LGAFC)	The blast response of clamped sandwich panels with layered-gradient aluminum foam cores was studied and the result show that all the layered-gradient core sandwich panels have a weaker blast resistance capability than the ungraded sandwich panels because of the reduction in the structural integrity of the specimens [23].
Li et al. (2021)	Air blast loading	Aluminum foam-cored sandwich plates	Experiments were firstly carried out to investigate the deformation and failure modes of aluminum foam-cored sandwich plates. The FE model indicated that the blast peak pressure was decreased during the propagation and was significantly increased when touching the front plate. The total energy absorption capability was increased while either increasing the explosive mass or decreasing the stand-off distance. In addition, the foamed core was prone to play a predominant role in energy absorption [11].
Liu et al. (2022)	Quasi-static compression load	U-type corrugated sandwich panel	The compression process can be divided into three stages. In stage I and stage II, the core panels are unstable and warp from the middle, and then the core panels are in contact with each other. In stage III, the core panels approach compaction [19].
Varghese (2022)	Blast loading	Woven and lattice core metallic sandwich panels	The analytical study on blast load response of triangular woven panels and pyramidal lattice panels of varying outer layer thicknesses. Pyramidal lattice panels show better performance than triangular woven panels [24].
Zhang (2022)	Blast loading	Steel plates with and without pre-formed holes	The effects of pre-formed holes on the deformation and failure of thin steel plates subjected to confined blast loading. Plates with preformed holes have smaller permanent displacement on the midpoint than an intact plate [25].

Several studies have been conducted to examine how the explosive loading scheme is applied to metal structures. However, several previous studies have not discussed the effect of differences in the honeycomb core compared to other geometries. Furthermore, there is no discussion on how to configure the nonlinear analysis configuration for the damaged model. Especially for the sandwich panel structure, we chose to study how the square and hexagonal honeycomb cores respond and vary with core height. In addition, the damaged model simulation was also carried out, and the results were analyzed. With this work, we endeavor to deepen the study on how it responds to blast loads. Thus, the sandwich structure was designed to withstand the given load with several configurations to optimize its function.

2.7. Methodology

The research was conducted in several stages. At the initial stage, a literature study was conducted on related research studies, followed by the sandwich panel design on the ABAQUS software. The design at this stage was carried out by replicating the design obtained from previous experiments. Then, we validated the experimental results with the results of the simulation. After obtaining the appropriate results, the research continued by changing the configuration of the core geometry, as well as the thickness of the honeycomb core. The geometries used were hexagonal and square, and the different thicknesses of the honeycomb core used were 31, 51, and 71 mm. The data obtained from the experiment are the value of the deflection that occurs in the sandwich panel in each variation. This research was carried out following the steps shown in Figure 5.

3. Benchmark and Mesh Strategy

Before this study was conducted to optimize the geometry and material of the sandwich panel, the simulation results were validated with experimental results related to Dharmasena et al. [4]. The results of the study in the form of deflection of the top plate and bottom plate showed a similar trend. However, it can be seen that there is a difference in the value of the deflection that occurs. This different result can occur due to differences in boundary conditions, wherein shifts in boundary conditions during the experiment may occur in real experiments. The difference in deflection values can also be caused by weak bonding between the plate and the sandwich core, causing them to lose connection. By assuming their different boundary conditions, this simulation can still continue to the honeycomb sandwich panel simulation under blast load.

Due to the symmetrical shape of the sandwich panels, only a quarter of the honeycomb sandwich structure was modeled. It can minimize system memory storage and reduce analysis computation time. The boundary conditions of the honeycomb sandwich panels were applied according to the designed symmetry conditions.

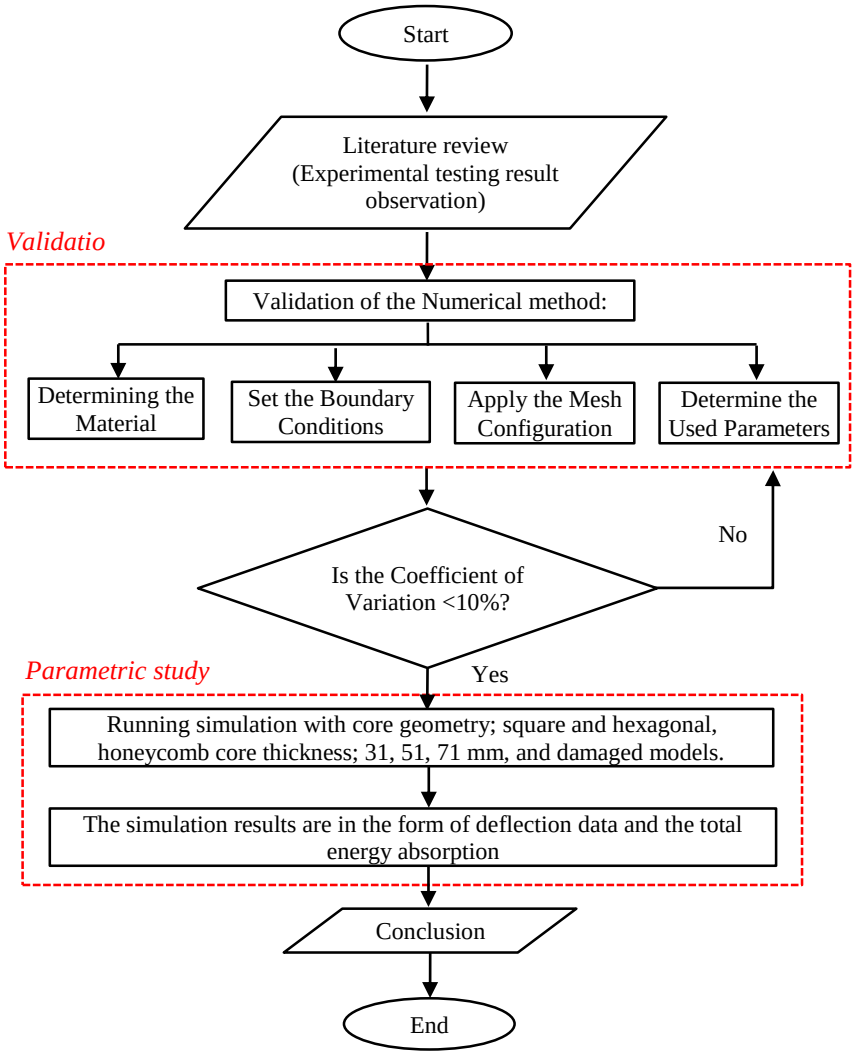

Figure 5. Flowchart for this research methodology

3.1. Experiment Profile

The honeycomb sandwich panel was designed with two solid plates as stiffeners and a honeycomb core located between the two stiffener plates. The test was carried out with a square honeycomb geometry as the core of the sandwich panel (Figure 6), which was based on the experimental work carried out by Dharmasena et al. [4]. In this experiment, the dimensions of the sandwich panels used were 610 × 610 mm. The top and bottom plates used as stiffeners had a thickness of 5 mm. The core had a height of 51 mm and a cell wall thickness of 0.76 mm for each lattice with a spacing between lattices of 30.5 mm.

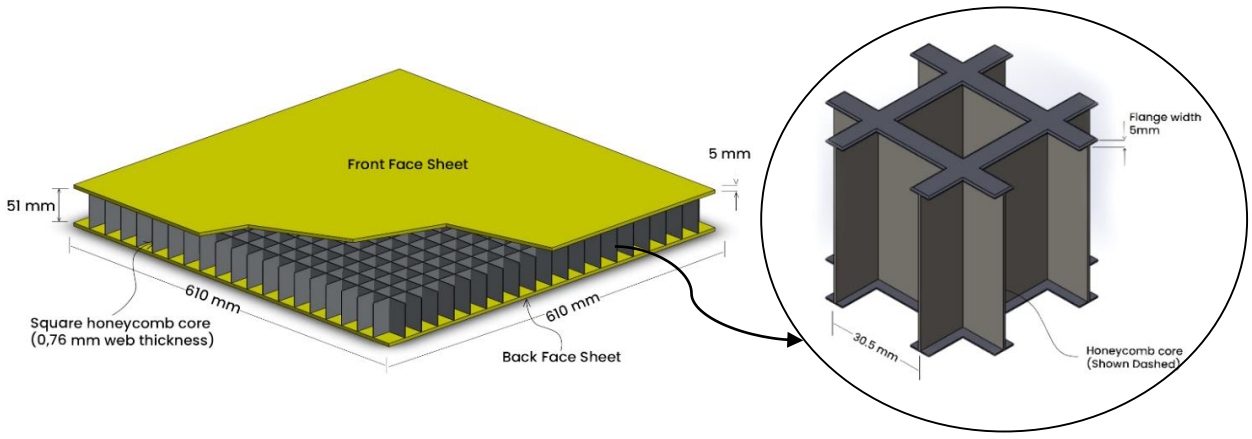

Figure 6. Dimension of sandwich panel structure based on a reference experiment [4]

The top side of the honeycomb core was connected to the inner surface of the front stiffener plate using the tie constraints found on the ABAQUS/CAE software menu panel. This constraint is used to prevent relative displacement between the surface of the stiffener plate and the honeycomb core. The connection between the core body and the stiffening plate was modeled using several welded joints. The welding process was carried out on the stiffening plates on the inner surface and the top and bottom of the honeycomb core. In addition, welded joints were also installed on the sides of the upper and lower stiffening plates with support beams that function as clamps when explosion testing is carried out. The bonding scheme between the honeycomb net, front plate, back plate, and support beams for clamping the sandwich panel structure is shown in Figure 7.

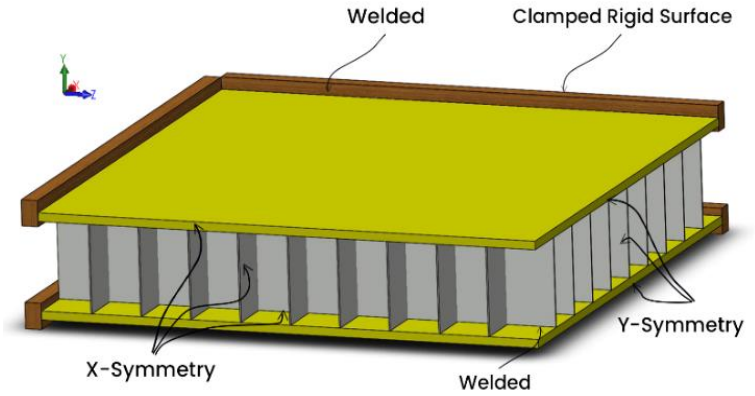

Figure 7. The boundary conditions scheme re-drawing based on reference [4]

3.2. Meshing Strategy

The mesh arrangement in the sandwich structure model used 31×31×5 mm eight-point Continuum-3D solid element with reduced integration (C3D8R) on the front and back plates. Then, at the honeycomb core height, we used 30 four-point bilinear shell elements with reduced integration (S4R). Each shell element used a five-point integration section according to Simpson's integration rules.

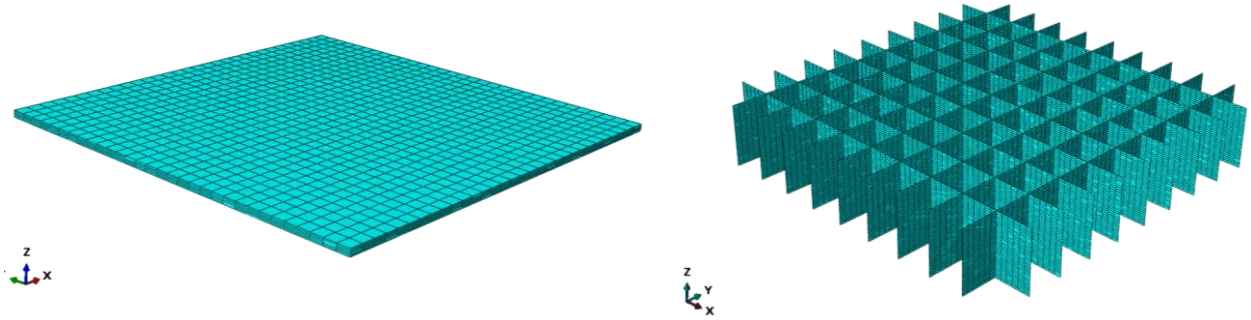

(a) (b)

Figure 8. Mesh configuration for sandwich panel structure. (a) Stiffener plate, (b) honeycomb core

To display the animation of the plate when it is deformed when subjected to an explosion load, the time period used was 1.5 ms. In this period, the plate goes through a compression process, as mentioned by Liu et al. [19]. In stages I and II, the honeycomb core undergoes unstable deformation, and the panels bend and press against each other. In stage III, the core panels approach compaction and the plastic phase occur. In the experiment, the stiffening plate was connected to the honeycomb core by the brazing technique.

3.3. Benchmarking Result

Validation of the simulation using the ABAQUS/CAE software was carried out by comparing the experimental results obtained in the research conducted by Dharmasena et al. [4]. The sandwich panel structure modeling is based on the geometry and size used in the experiment. The dimensions of the sandwich panels used were 610 × 610 mm. The two stiffener plates at the top and bottom of the panel had a thickness of 5 mm. The sandwich panel core was 51 mm high and had a cell wall thickness of 0.76 mm for each lattice with a spacing between lattices of 30.5 mm.

A comparison of experimental and numerical results on variations in blast loads of 1 kg, 2 kg, and 3 kg TNT seen from the front face deflection and back face deflection is shown in Figure 9.

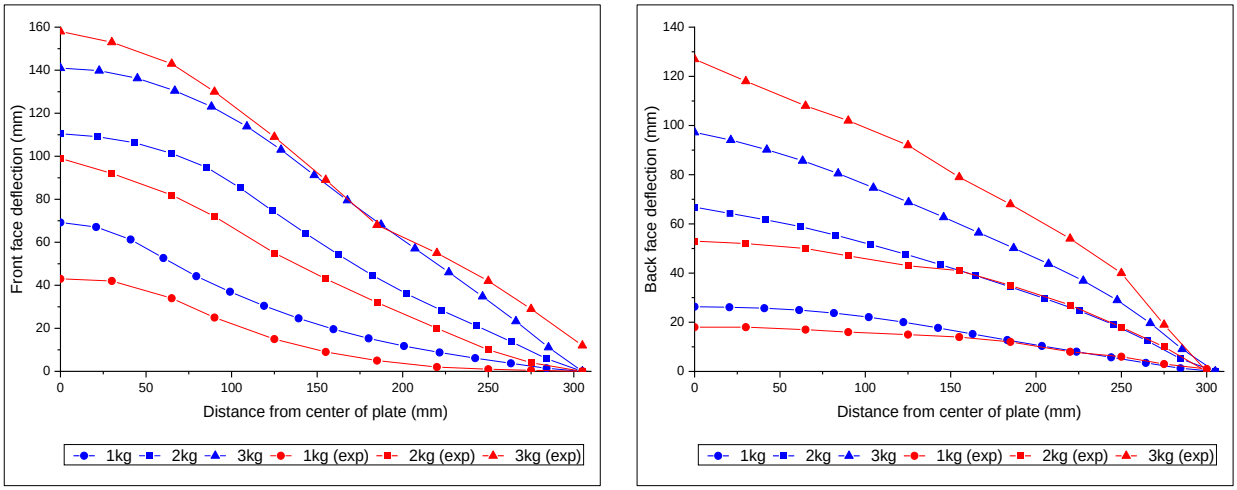

(a) (b)

Figure 9. Comparison of experimental and numerical results of front face deflection vs. distance from the center of plate: (a) front face, (b) back face

4. FE Configuration and Setting

We modeled the square and hexagonal core geometries using ABAQUS/CAE with reference sizes based on the experimental profile in Section 3.1. Sandwich panel models with a square and hexagonal core are shown in Figure 10.

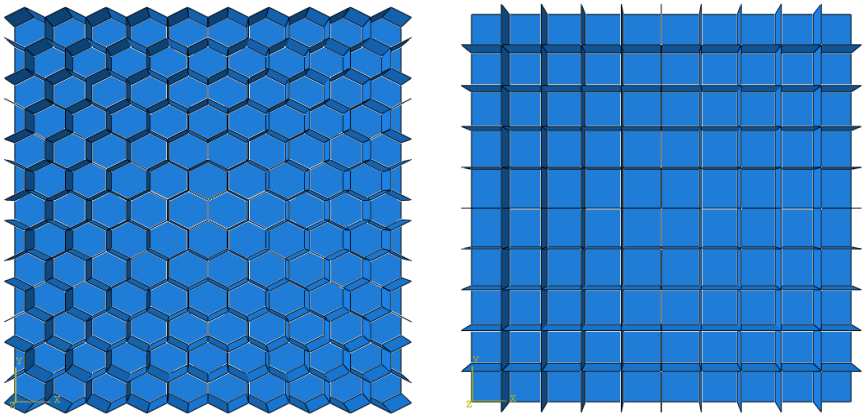

(a) (b)

Figure 10. Honeycomb core geometry model generated by ABAQUS/CAE: (a) hexagonal geometry, (b) square geometry

In the experimental profile, the upper and lower stiffener plates are modeled with a size of 610 × 610 mm with a thickness of 5 mm. Due to the symmetry conditions in the simulation, only a quarter of the sandwich panel structure is modeled. The honeycomb model on ABAQUS/CAE software was 305×305 mm with a plate thickness of 5 mm. Square and hexagonal honeycomb cores have an equivalent in length for each shell of 30.5×30.5 mm. Figure 11 shows the dimensions of each shell core of the sandwich panel.

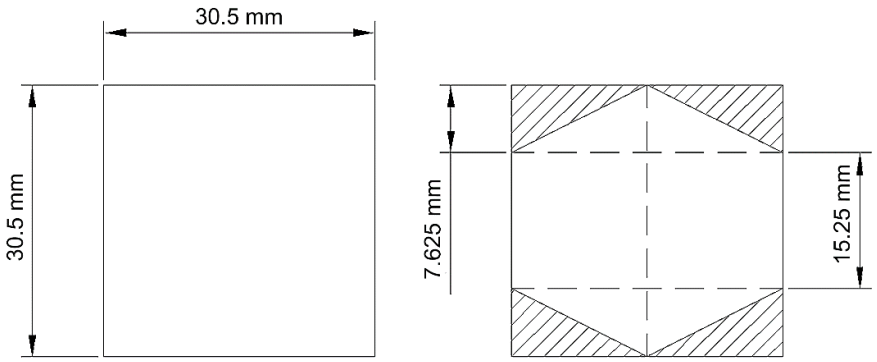

Figure 11. Dimensions of honeycomb core geometry: (a) hexagonal geometry, (b) square geometry

4.1. Intact Model of Sandwich Structure

Figure 12 shows the deformation reference point for the intact honeycomb sandwich panel model. In the figure, the deflection measurement reference point is taken at the point where the sandwich panel has not been damaged.

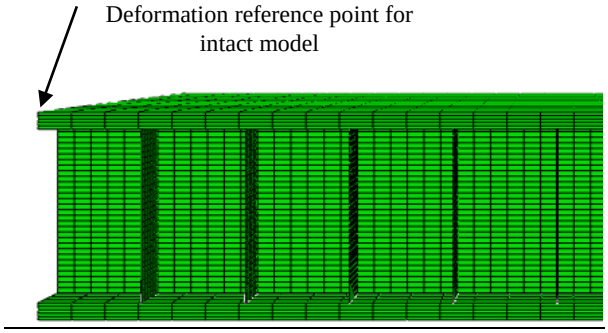

Figure 12. Deformation reference point for the intact honeycomb sandwich panel model

4.2. Damaged Model of Sandwich Structure

Figure 13 shows the deformation reference point for the damaged model honeycomb sandwich panel. The reference point for the deflection measurement is taken at the point after the dent damage occurs on the sandwich panel.

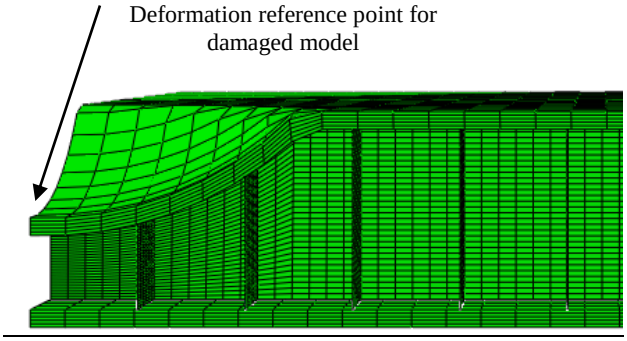

Figure 13. Deformation reference point for the damaged model honeycomb sandwich panel

4.3. Material and Failure Definition

The materials used to make honeycomb sandwich panels are stainless steel alloys (AL6XN). The material behavior is modeled using the Johnson–Cook (JC) model [2]. The Johnson-Cook material model is a semi-empirical constitutive model that describes the plastic behavior at strain, strain rate, and high temperatures. Using the Johnson–Cook model, the flow voltage can be expressed as:

$$\sigma = (A + B\varepsilon^n)\left[1 + C\ln\left(\frac{\dot{\varepsilon}}{\dot{\varepsilon}_0}\right)\right]\left[1 - \left(\frac{T - T_{room}}{T_{melt} - T_{room}}\right)^m\right]. \quad (10)$$

where σ is the material flow stress, ε is the plastic strain, $\dot{\varepsilon}$ is the strain rate, and $\dot{\varepsilon}_0$ is the reference strain rate. T is the temperature of the material, T_{melt} is the material's melting point, and T_{room} is the room temperature. The empirical constants are as follows: A is the yield stress, B is the pre-exponential factor, C is the strain rate factor, n is the work-hardening exponent, and m is the thermal softening exponent [26]. The Johnson–Cook constants for the stainless steel alloy (AL6XN) are shown in Table 2.

Table 2. Johnson–Cook parameters for SS alloy (AL6XN)

Johnson–Cook Parameter	SS Alloy (AL-6XN)	Unit
A	400	MPa
B	1500	MPa
N	0.4	-
M	1.2	-
Tm	1527	(°C)
T0	20	(°C)
C	0.045	-
$\dot{\varepsilon}$	0.001	-

We designed square and hexagonal sandwich panels using elastic properties such as the density of material, Young's modulus, and Poisson's ratio. Table 3 shows the material properties of AL6XN.

Table 3. Material properties for SS alloy (AL6XN)

Material Properties	SS Alloy (AL-6XN)	Unit
Density	400	(g/mm^3)
Young's Modulus	161	GPa
Poisson's Ratio	0.35	-

4.4. Load and Boundary Conditions

Since the simulation and analysis process of sandwich panel design is in a symmetrical condition both in the structure and under loading conditions, the boundary condition modeling must also adjust the position when the structure is cut into four parts. The joint section defined as rigid is on the outer side of the top and bottom plates, while the honeycomb structure section is determined using x-symmetry and y-symmetry. Figure 14 shows the boundary condition modeling scheme performed on ABAQUS/CAE software.

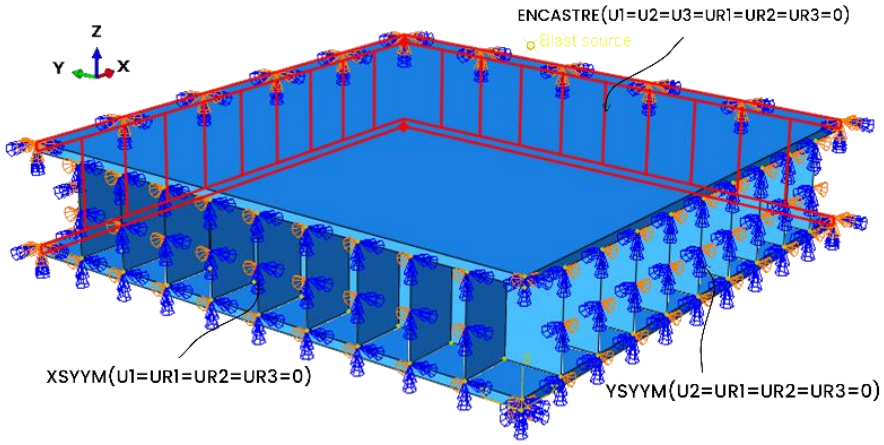

Figure 14. The boundary conditions model generated by ABAQUS/CAE software

The limits on the outside are set for all degrees of motion (ENCASTRE). The condition of symmetry about the x-axis (XSYMM) is applied to the plane in the direction of the y-axis (x=0). Similarly, symmetry conditions about the y-axis (YSYMM) are applied to the plane parallel to the x-axis (y=0). The center of air blast loading is placed at a standoff distance of 100 mm from the square front plate and hexagonal honeycomb core panels. The mass of the detonated TNT was 1, 2, and 3 kg. For the intact model, Figure 15-a shows the distance of the blast source to the intact model sandwich structure. Figure 15-b shows the distance between the center of the explosion to the damaged sandwich panel structure. The dents were modeled by making the center of the structure hollow. The depth of the dent was 30 mm. The simulation results are compared with the experimental results to ensure that the sandwich panel modeling performed on the software follows the treatment given in the explosion test experiment.

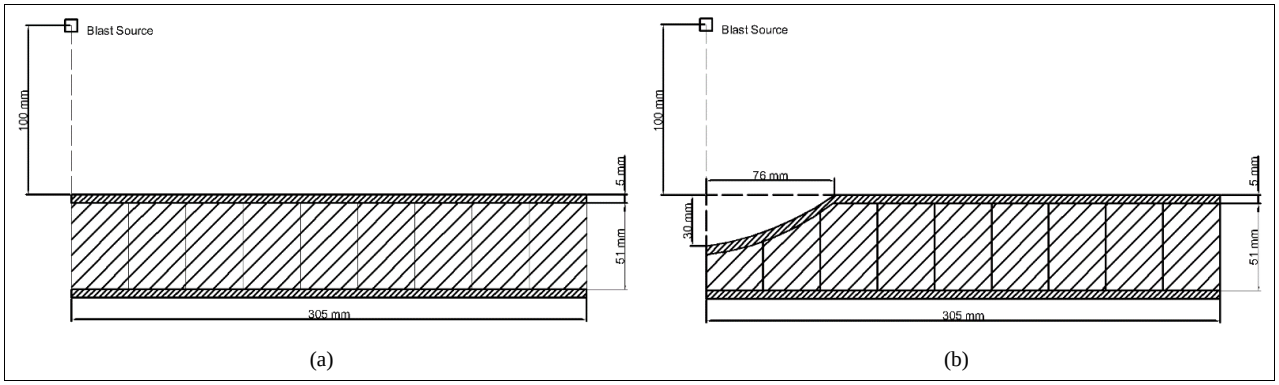

Figure 15. Standoff distance of blast source to the sandwich structure: (a) intact model, (b) damaged model

5. Parametric Study

5.1. Comparison of Square and Hexagonal Honeycomb Core

The material used for Finite Element Simulation in the structure is a stainless steel alloy (AL6XN). Geometric variation is used to see the difference in deformation. The graph shows two different line colors. The red line shows the shape of the square honeycomb core, and the blue line shows the geometric hexagonal core. The explosion simulation code can calculate the pressure distribution and impulse loading due to the explosion load on the sandwich panel surface. The results show that the difference in the geometric shape of the honeycomb core can affect the panels' strength in reducing the plate's deflection. Figure 16 shows graphs comparing deflection values in square and hexagonal honeycomb cores.

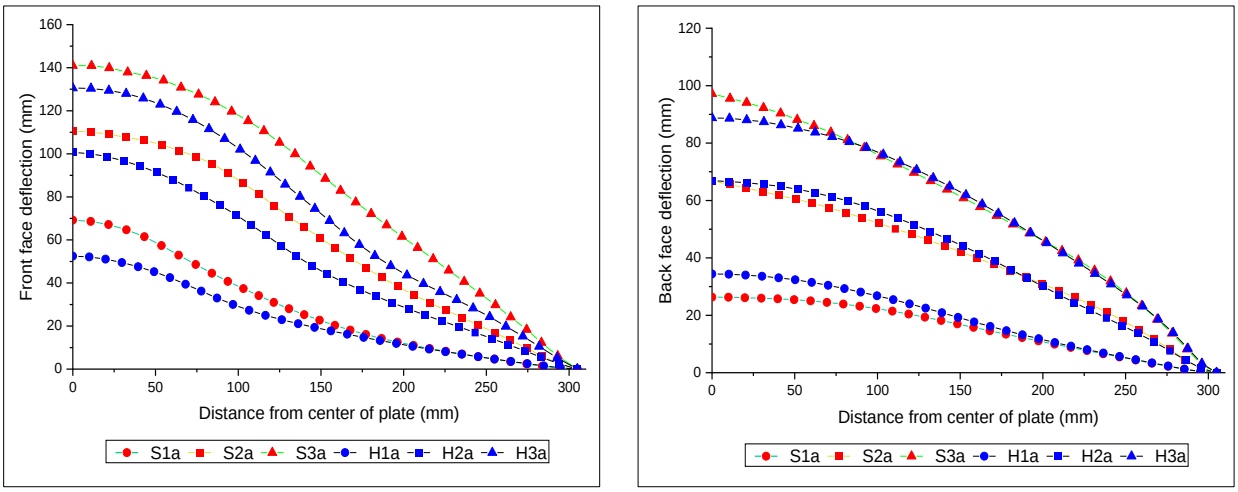

(a) (b)

Figure 16. Comparison of the numerical results of square and hexagonal honeycomb core

The geometry used to compare the square honeycomb core is a hexagonal shape. All dimensions used follow experimental models carried out previously and have a comparable width of 30.5 mm. Both core shapes were tested by appropriate modeling and simulation procedures, with blast loads of 1, 2, and 3 kg TNT. Finally, the deflection value was obtained and analyzed. The codes used in the graph legend are H1a, H2a, H3a, S1a, S2a, and S3a, which indicate the type of variation used. The first letter represents the honeycomb core geometry, i.e., H for hexagonal and S for Square. The numbers indicate the mass of TNT used, and the last letter indicates the material used in this simulation, which is a stainless-steel alloy (AL6XN). The graph shows significant differences in plate deformation values where the sandwich panel model using a square honeycomb core has a higher deflection value. Otherwise, honeycomb cores with hexagonal geometry tend to be better suited to withstand blast loads and reduce deflection values in the plate.

The front face deflection values for the square honeycomb core are 141, 110, and 69 mm. At the same time, the rear face deflection values are 97, 67, and 26 mm. The deflection of the hexagonal honeycomb showed lower values for different blast loads of 3 kg TNT, 2 kg TNT, and 1 kg TNT. The front face deflection values are 130, 101, and 52 mm, respectively. Similarly, the sandwich panel deflections for the same blast load show that the rear face deflections are 88, 66, and 34 mm, respectively. Figure 17 shows the simulation results of the ABAQUS/CAE software on a square honeycomb core. Figure 17-a shows the resulting deformation when the mass of TNT is 1 kg, Figure 17-b when the mass of TNT is 2 kg, and Figure 17-c when the mass of TNT is 3 kg.

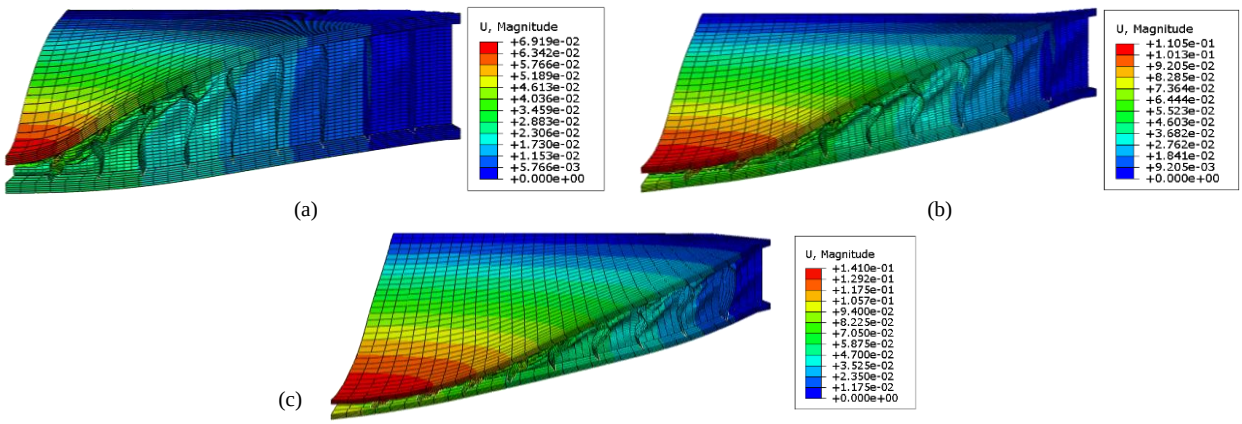

(a) (b) (c)

Figure 17. Deformation of hexagonal honeycomb at mass of TNT (a) 1 kg, (b) 2 kg, and (c) 3 kg

The deformation phenomenon seen in Figure 17a shows that the plastic deformation of the honeycomb core is dominant; besides that, there is also a bending behavior of the plate. Figure 17b shows the honeycomb core undergoing shear deformation and slab stretching behavior. Figure 17c shows the effects of crushing, slab stretching, and deboning of the face plate. The most significant deformation is shown at the blast load of 3 kg TNT. There is a deboning effect on the front and back plates. It causes some of the back plates to bend. More significant damage between the front plate and the honeycomb core can weaken the overall strength of the plate. As a result, the back plate is also subjected to large deformations.

When subjected to a blast load of 3 kg of TNT, it is seen that the honeycomb core begins to collapse and cannot withstand the blast ware pressure pulse, so it presses on the front plate and damages the honeycomb core arrangement. Almost all of the back plate is also subject to considerable deflection, although the deflection is less than in the square honeycomb core. The ability of the hexagonal honeycomb core to withstand loads means the damage that occurs to the panels can be minimized so that there is no shear deformation in the structure. Thus, a comparison of the deformations occurring in the two geometries of the honeycomb core has been obtained. Next, we observed how the damaged model responds with a dent in the center of the structure to blast loading.

5.2. Deflection Behavior of Intact and Damaged Model

The explosion response characteristics that occur in the intact and damaged models show the same trend. Figures 18 to 20 show graphs of face deflection over time for the front and back faces of the sandwich panels. It can be seen that the test on the damaged model shows lower deflection results than the intact model. The difference that occurs can also be because the system in the ABAQUS/CAE software by default takes the deflection reference point on the surface of the object, where the surface damage structure has a dent as deep as 30 mm.

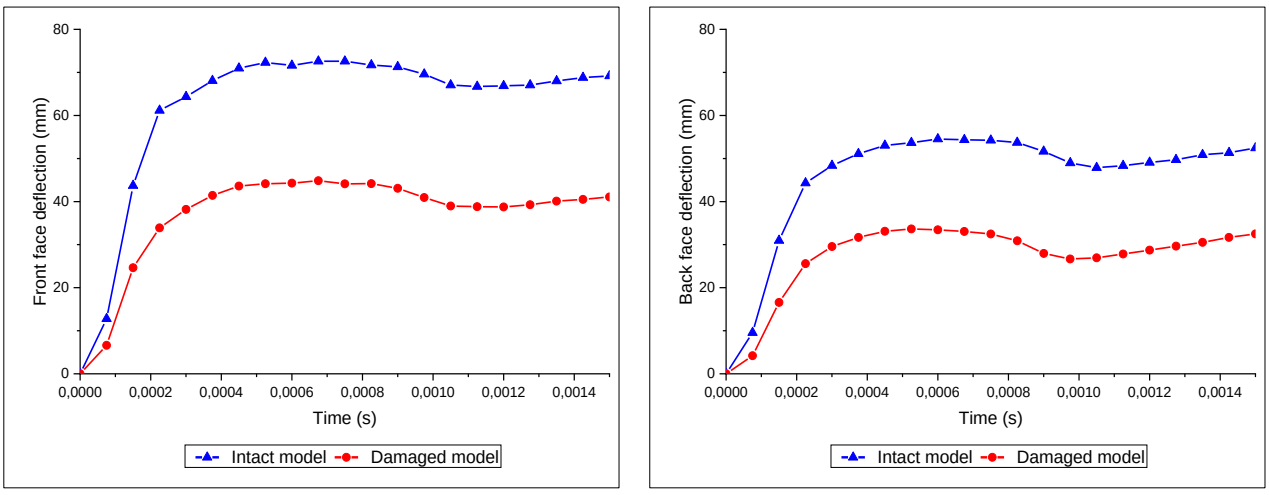

(a) (b)

Figure 18. Comparison of deflections in intact and damaged models for a load of 1 kg TNT: (a) front face, (b) back face

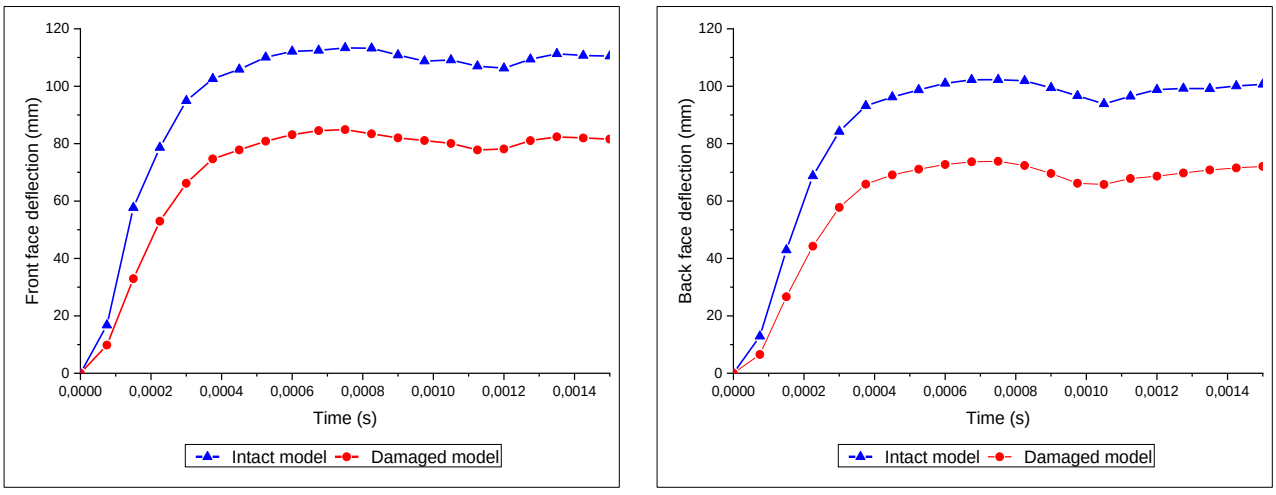

(a) (b)

Figure 19. Comparison of deflections in intact and damaged models for a load of 2 kg TNT: (a) front face, (b) back face

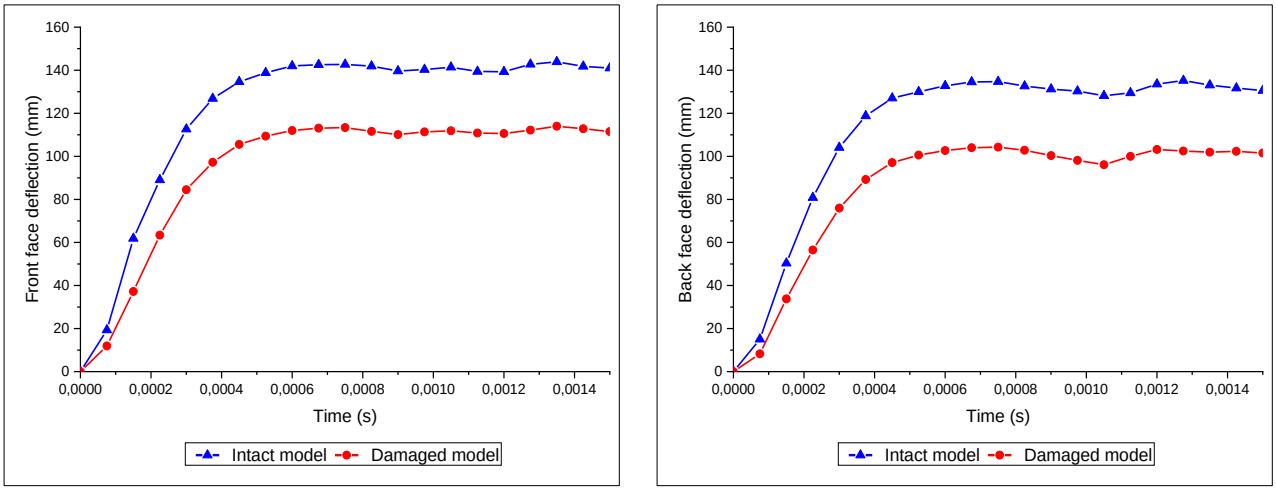

(a) (b)

Figure 20. Comparison of deflections in intact and damaged models for a load of 3 kg TNT: (a) front face, (b) back face

Figure 21 shows the results of the ABAQUS/CAE software simulation on the damaged sandwich structure model. Figure 21-a shows the resulting deformation when the mass of TNT is 1 kg, Figure 21-b when the mass of TNT is 2 kg, and Figure 21-c when the mass of TNT is 3 kg.

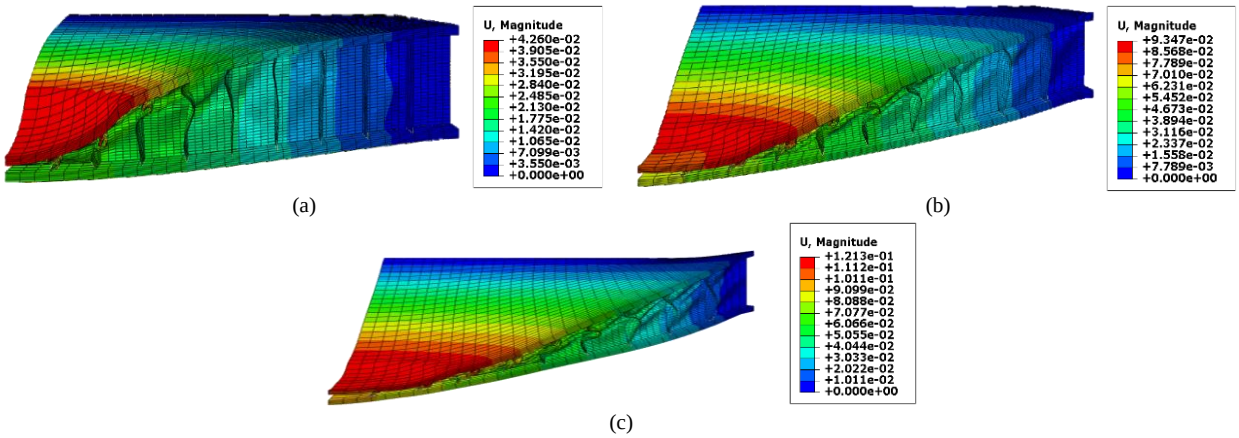

(a) (b)

(c)

Figure 21. Deformation of damaged structure honeycomb sandwich panel of TNT: (a) 1 kg, (b) 2 kg, and (c) 3 kg

5.3. Investigation of Different Core Height in Sandwich Structure

The thickness of the honeycomb core greatly affects the structure's strength in resisting deflection. In this study, several simulations were carried out using three models of honeycomb core height, 31, 51, and 61 mm. Using the same modeling and simulation procedures, these models are compared as they are subjected to 1 kg, 2 kg, and 3 kg of TNT. The designs of each model created in ABAQUS/CAE are shown in Figure 22.

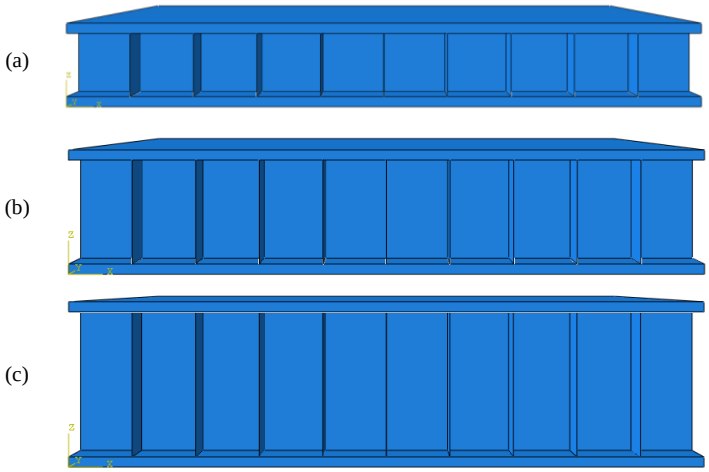

(a)

(b)

(c)

Figure 22. Deformation of damaged structure honeycomb sandwich panel of TNT: (a) 1 kg, (b) 2 kg, and (c) 3 kg

The simulation results show that the deflection decreases as the height of the honeycomb core increases. It means a honeycomb core with a higher core height will be more optimal in resisting deformation. However, effectiveness and other factors must be considered. Figures 23 and 24 show the deflection values that occur in the front and back face for square and hexagonal core sandwich panels with various heights of the cores when subjected to blast loads.

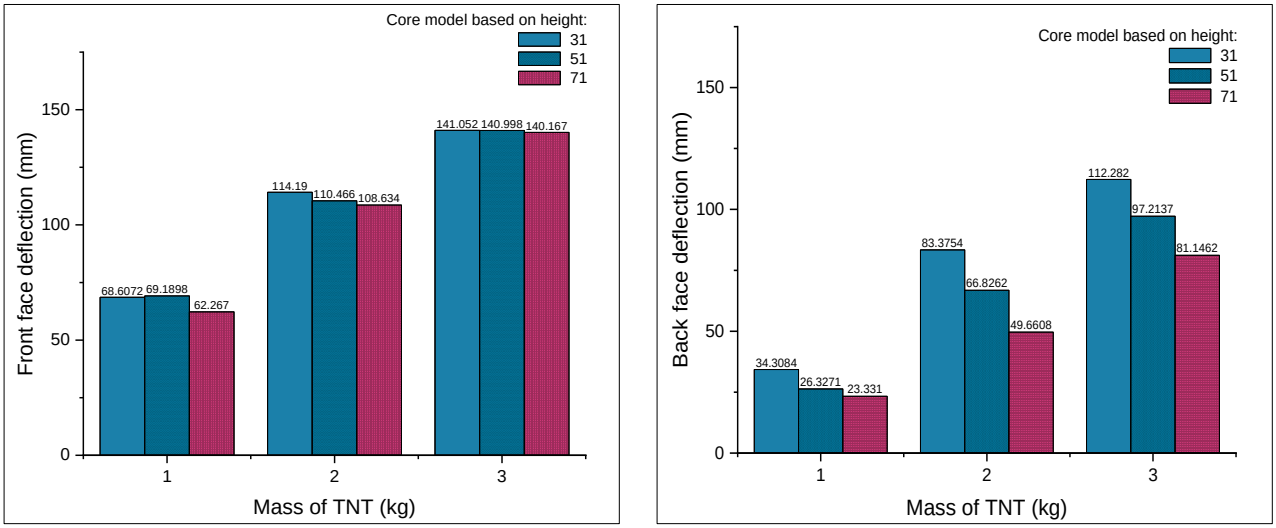

(a) (b)

Figure 23. Graph of deflection on square honeycomb with various core heights: (a) front face, (b) back face

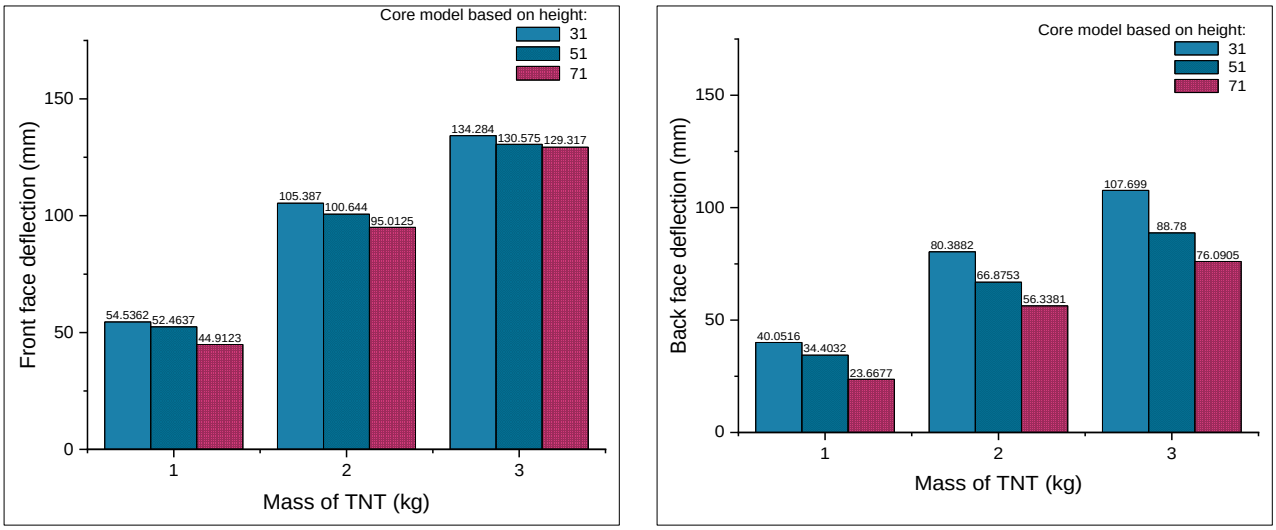

(a) (b)

Figure 24. Graph of deflection on hexagonal honeycomb with various core heights: (a) front face, (b) back face

The hexagonal core model also still shows the same trend: the strength of the structure in resisting deflection is higher if the structure has a higher core height. Figure 25 shows that significant nuclear disintegration occurs for enormous masses. For example, when subjected to a TNT load of 3 kg, the maximum compressive strain has a value of 0.14. The process required for the sandwich structure to reach maximum deflection occurs very quickly, in less than 0.4 ms. After receiving the shock load, the sandwich panel structure will respond with elastic properties before the structure turns into plastic. At that time, the phenomenon of "*spring-back*" also occurs before the structure gives a permanent response. When subjected to a load of 2 kg, the crushing process occurs in a shorter time than when the mass of TNT is larger. Loading of 1 kg of TNT also experienced the spring-back phenomenon, and the crushing process was completed in a short time, almost 0.2 ms.

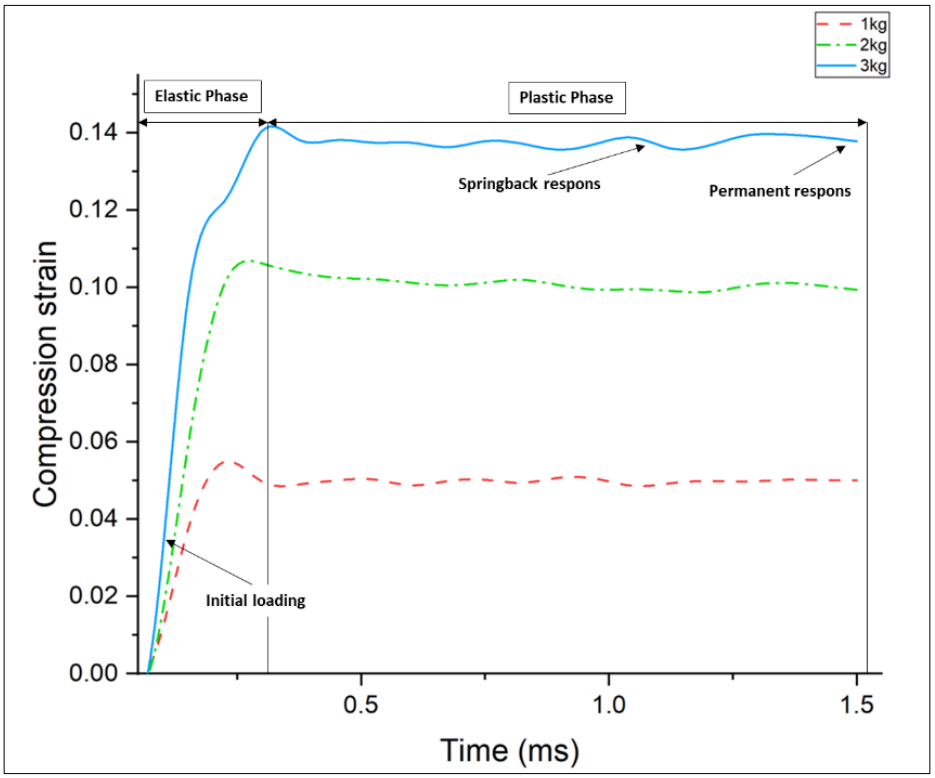

Figure 25. Time dependence of compressive strain obtained from ABAQUS/CAE simulation

5.4. Stress and Strain

According to Nemat-Nasser et al. [27], the experimental results of Al-6XN stainless steel reveal some characteristics that need to be addressed in plastic deformation modeling. The plastic deformation of the AL-6XN stainless steel is calculated using the secant modulus defined by Farid et al. [28]. Figure 26 shows isothermal stress–strain curves predicted by the proposed model for AL-6XN stainless steel. The plastic deformation of stainless steel AL-6XN was calculated using the secant modulus. The calculation results were compared with experimental results obtained for low and high strain rates and temperatures. There is a good correlation between the results predicted by the proposed model and the experimental results presented by Nemat-Nasser [27]. In this study, the phenomenon of stress–strain on AL-6XN material was obtained when subjected to an explosion load.

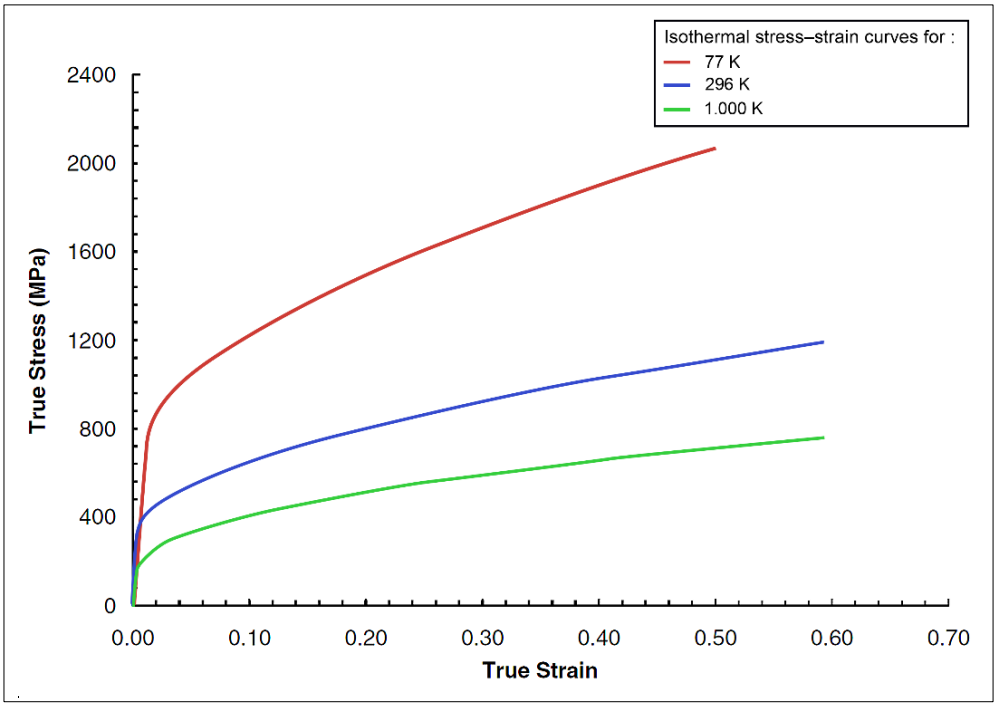

Figure 26. Isothermal stress–strain curves predicted by the proposed model for AL-6XN stainless steel [24]

5-4-1- Stress Behavior

In this method, output stresses were generated. ABAQUS/CAE software was used to assess von Mises stress [29-35]. AL6XN material is used to show the result of the stress contour. Then, the stress values were extracted from the analysis file to generate stress contour. Figure 27 shows the comparison of von Mises stress on the square and hexagonal honeycomb geometry with AL-6XN material.

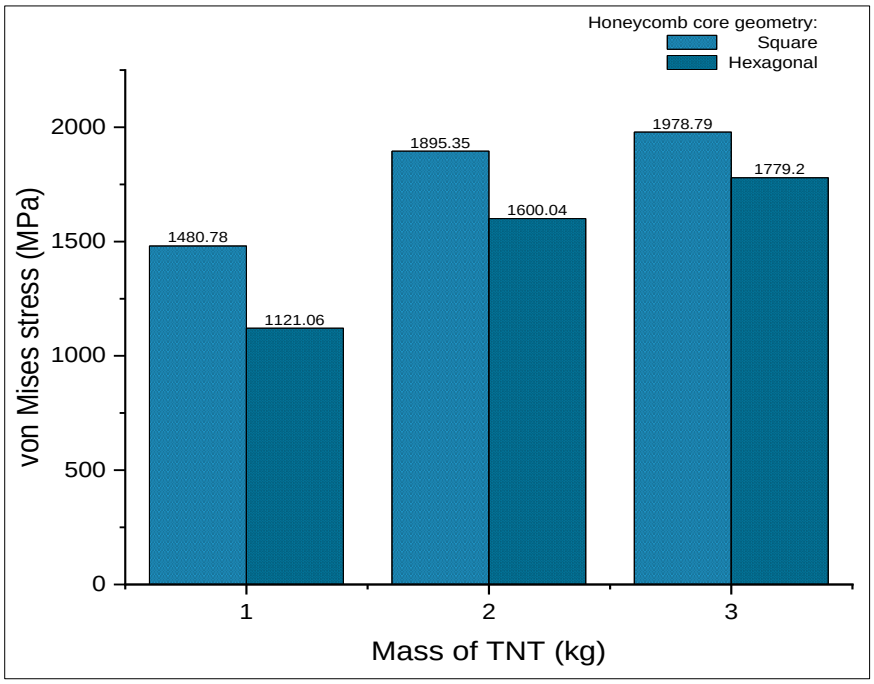

Figure 27. Von Mises stress graphs of AL-6XN exposed to blast loads

Based on a study conducted by Alabdullah [36], it is known that the AL-6XN alloy requires a high strain to yield due to its high tensile strength. The graph in Figure 27 identifies the stress behavior when the sandwich panel structure is subjected to TNT loads of 1 kg, 2 kg, and 3 kg. Then, the stress results are compared to the two honeycomb core geometries. There is a square and hexagonal honeycomb. On the square honeycomb core geometry, the effects of the von Mises stress are higher than in the hexagonal core. The maximum value of von Mises stress occurred in the front plate of square honeycomb variation with a TNT load of 3 kg, reaching 1978.79 MPa. At 2 kg and 1 kg TNT loads, the stress values tend to be lower, 1895.35 MPa and 1480.78 MPa, respectively. The significant difference in von Mises stress values occurs in the front plate of hexagonal core geometry, where for loads of 1 kg, 2 kg, and 3 kg, the stress occurs at 1779.2 MPa, 1600.04 MPa, and 1121.06 MPa, respectively. Figures 28 to 31 show the plastic strain results in the blast load simulation.

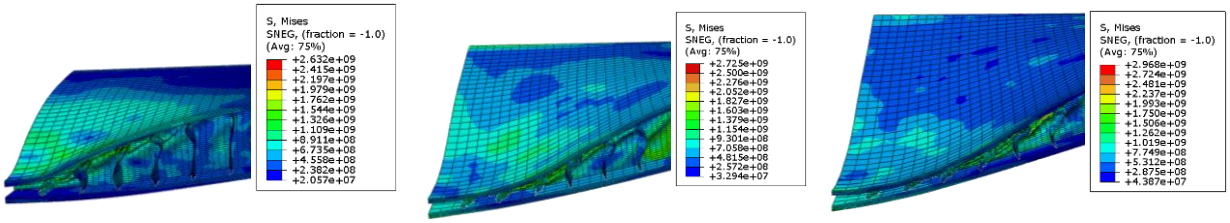

Figure 28. Von Mises stress for square honeycomb core sandwich structure

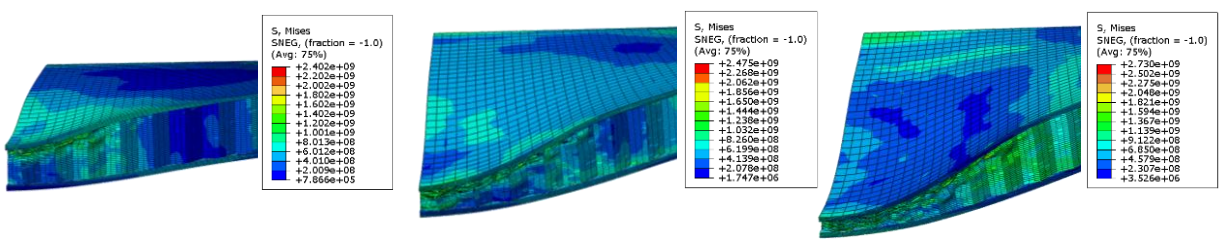

Figure 29. Von Mises stress for hexagonal honeycomb core sandwich structure

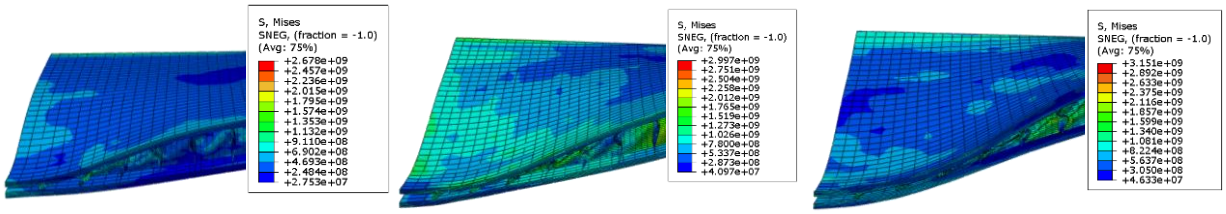

Figure 30. Von Mises stress for square honeycomb core sandwich structure with 31 mm core height

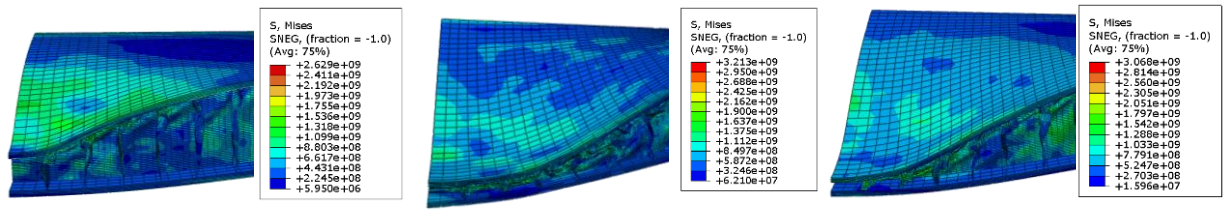

Figure 31. Von Mises stress for square honeycomb core sandwich structure with 71 mm core height

5-4-2- Strain Behavior

Based on the plastic strain contour, it can be observed that the honeycomb structure is not subjected to heavy strain. This state is indicated by the honeycomb edges in blue and green, indicating that the element does not experience significant strain, or can be expressed as a minimum deformation. Figure 32 shows the comparison of PEEQ plastic strain on the square and hexagonal honeycomb geometry with AL-6XN material.

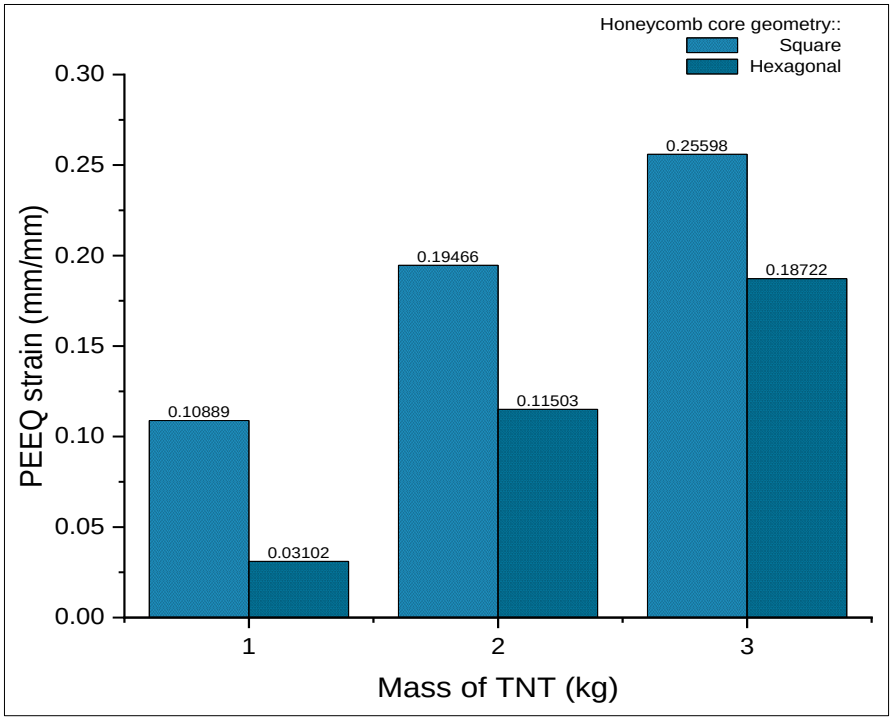

Figure 32. PEEQ strain graphs of AL-6XN exposed to blast loads

The graph in Figure 32 identifies the plastic strain behavior when the sandwich panel structure is subjected to TNT loads of 1, 2, and 3 kg. Then, the strain results that occur are compared to the two honeycomb core geometries, square and hexagonal. The results obtained on the square honeycomb core geometry are higher strains than the hexagonal core. PEEQ values of plastic strain on the front plate of a square honeycomb with TNT loads of 1, 2, and 3 kg reached 0.11, 0.19, and 0.26, respectively. Significant differences in strain values occurred in the front plate of the hexagonal core geometry, where for loads of 1, 2, and 3 kg, the stresses were 0.03, 0.11, and 0.19, respectively. Figures 33 to 36 show the PEEQ plastic strain distribution on the sandwich panel after the blast load simulation.

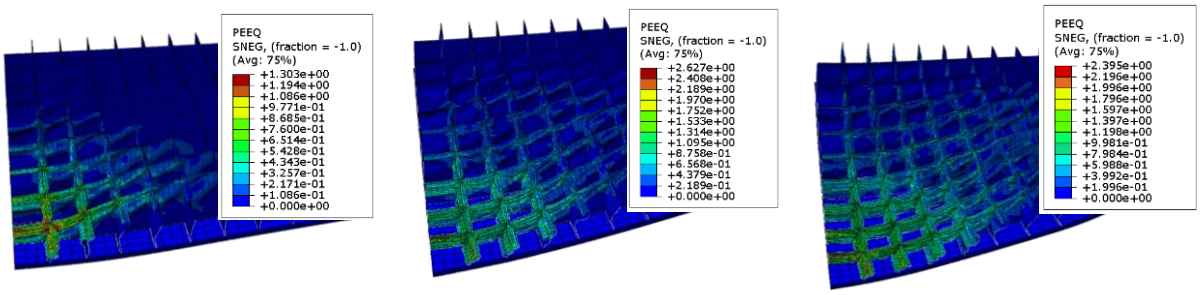

Figure 33. PEEQ strain for square honeycomb core sandwich structure

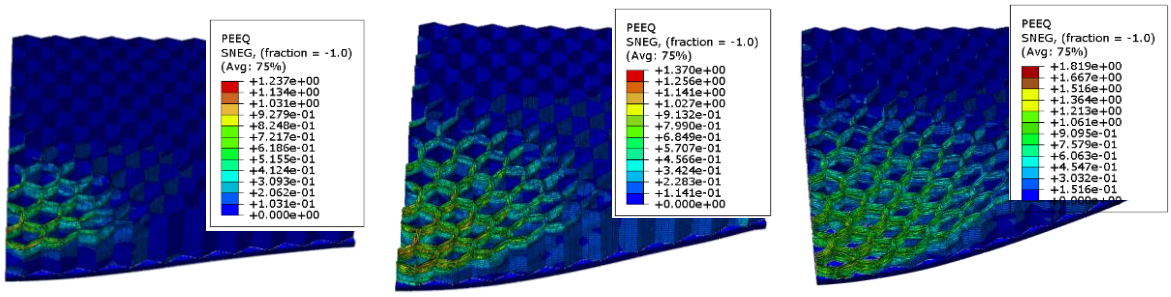

Figure 34. PEEQ strain for hexagonal honeycomb core sandwich structure

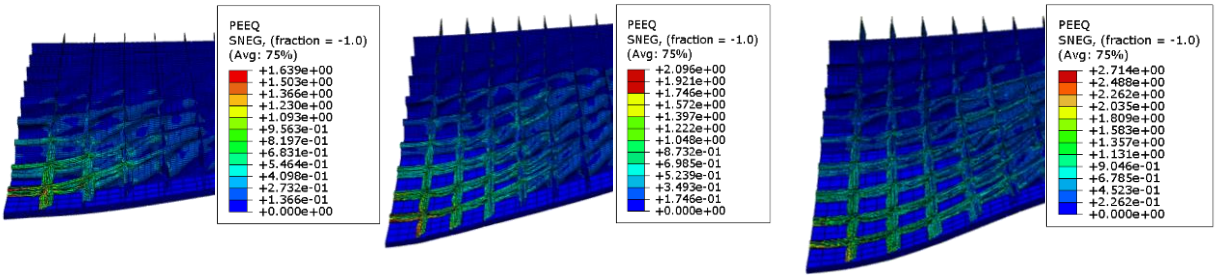

Figure 35. PEEQ strain for square honeycomb core sandwich structure with 31 mm core height

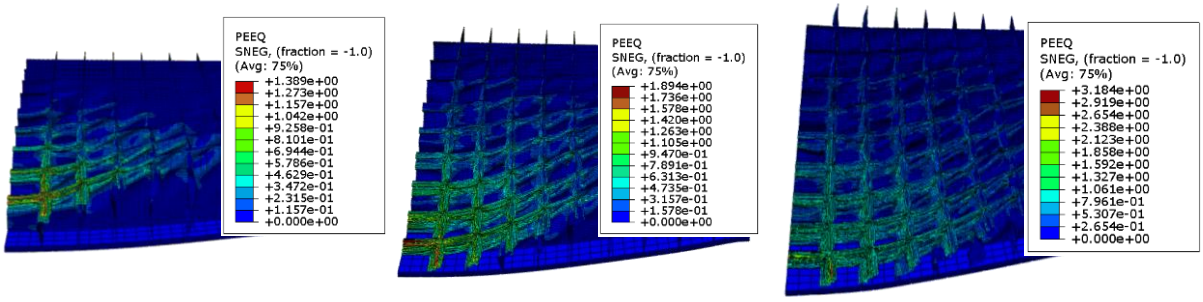

Figure 36. PEEQ strain for square honeycomb core sandwich structure with 71 mm core height

6. Conclusions

In this study, we show that the use of a honeycomb sandwich panel structure as a means to increase the structural resistance to blast loads is attractive. The performance of the structure is effective in minimizing the damage that occurs. A sandwich panel structure was made using stainless steel alloy material (AL6XN). Simulations were carried out using variations of square and hexagonal sandwich panel cores at different core heights, i.e., 31, 51, and 71 mm. In addition, we also investigated how the response of the damaged honeycomb structure compared to that of the intact model. We obtained several conclusions, as follows:

- The use of a hexagonal core is proven to be more effective in holding loads and reducing deflection of the sandwich plate, where the maximum deflection at a TNT load of 3 kg is 130 mm. The square honeycomb core experienced a maximum deflection of 141 mm.
- The height of the honeycomb core is also an influential factor in structural damage. A honeycomb core that has a higher core height will reduce the deflection that occurs in the plate. These results indicate that the plate with the larger core height has significant energy absorption.

- Structural strength is also affected by damage. The results from the damaged model show that its strength in resisting plate deformation is not better than that of the intact structure.
- The core compressive strain is calculated at the center of the panel as a function of time for each applied impulse. Maximum core destruction occurs at high-intensity loads. The maximum core compressive strains are 0.13, 0.09, and 0.05 for TNT loads of 3, 2, and 1 kg, respectively.
- The stainless-steel alloy (AL-6XN) material requires high strain to yield due to its high tensile strength. The maximum values of von Mises stress occurring on the front plate of the square honeycomb variation reached 1978.79, 1895.35, and 1480.78 MPa for TNT loads of 3, 2, and 1 kg, respectively.
- The PEEQ value of plastic strain on the geometry of the square honeycomb core was greater than the hexagonal core. On a square honeycomb front plate with TNT loads of 1, 2, and 3 kg, the strains reached 0.11, 0.19, and 0.26, respectively. On the front plate of the hexagonal core geometry, for loads of 1 kg, 2 kg, and 3 kg, the strain values were 0.03, 0.11, and 0.19, respectively. Significant differences in strain values occur in the two sandwich panel core geometries.

The optimization of the strength of the sandwich panel structure with several configurations was achieved in this work. However, in its implementation, it is still necessary to consider other production factors such as material weight, costs, and other parameters that affect the sandwich panel structure design. The study of the influence of honeycomb core geometry is not limited to hexagonal and square shapes. Many other core geometry models can represent future research opportunities to create sandwich panel structures with better performance. Finally, the application of sandwich panel structures to replace conventional plates can be considered for component manufacturing in various sectors, such as automobile, aerospace, and defense applications.

7. Declarations

7.1. Author Contributions

Conceptualization, D.T.A.A., A.R.P., T.M., and F.B.L.; Methodology, D.T.A.A., A.R.P., N.M., and T.M.; Software, A.R.P., T.M., F.B.L., D.D.D.P.T., A.P. and Y.K.; Validation, A.R.P., T.M., and F.B.L.; Formal analysis, D.T.A.A., A.R.P., N.M., and T.M.; Investigation, D.T.A.A., A.R.P., T.M., N.M., and F.B.L.; Resources, A.R.P., T.M., F.B.L., D.D.D.P.T., A.P. and Y.K.; Data curation, D.T.A.A. and T.M.; Writing—original draft preparation, D.T.A.A., A.R.P., and T.M.; Writing—review and editing, D.T.A.A., A.R.P., and T.M.; Visualization, D.T.A.A. and A.R.P.; Supervision, A.R.P., T.M., N.M. and F.B.L.; Project administration, N.M., D.D.D.P.T., A.P. and Y.K.; Funding acquisition, N.M., D.D.D.P.T., A.P. and Y.K. All authors have read and agreed to the published version of the manuscript.

7.2. Data Availability Statement

The data presented in this study are available on request from the corresponding author.

7.3. Funding and Acknowledgements

This work was supported by the RKAT PTNBH Universitas Sebelas Maret Year 2022, under the Research Scheme of “Penelitian Unggulan Terapan” (PUT-UNS), with research grant/contract no. 254/UN27.22/PT.01.03/2022. The support is gratefully acknowledged by the authors.

7.4. Conflicts of Interest

The authors declare no conflict of interest.

8. References

[1] Liang, C. C., & Tai, Y. S. (2006). Shock responses of a surface ship subjected to noncontact underwater explosions. Ocean Engineering, 33(5–6), 748–772. doi:10.1016/j.oceaneng.2005.03.011.

[2] Soleimani, S. M., Ghareeb, N. H., & Shaker, N. H. (2018). Modeling, Simulation and Optimization of Steel Sandwich Panels under Blast Loading. American Journal of Engineering and Applied Sciences, 11(3), 1130–1140. doi:10.3844/ajeassp.2018.1130.1140.

[3] Kumar, R., & Patel, S. (2019). Failure analysis on octagonal honeycomb sandwich panel under air blast loading. Materials Today: Proceedings, 46, 9667–9672. doi:10.1016/j.matpr.2020.07.525.

[4] Dharmasena, K. P., Wadley, H. N. G., Xue, Z., & Hutchinson, J. W. (2008). Mechanical response of metallic honeycomb sandwich panel structures to high-intensity dynamic loading. International Journal of Impact Engineering, 35(9), 1063–1074. doi:10.1016/j.ijimpeng.2007.06.008.

[5] Xue, Z., & Hutchinson, J. W. (2006). Crush dynamics of square honeycomb sandwich cores. International Journal for Numerical Methods in Engineering, 65(13), 2221–2245. doi:10.1002/nme.1535.

[6] Yu, S., Yu, X., Ao, Y., Mei, J., Jiang, W., Liu, J., Li, C., & Huang, W. (2021). The impact resistance of composite Y-shaped cores sandwich structure. Thin-Walled Structures, 169, 108389. doi:10.1016/j.tws.2021.108389.

[7] Ma, J., Dai, H., Chai, S., & Chen, Y. (2021). Energy absorption of sandwich structures with a kirigami-inspired pyramid foldcore under quasi-static compression and shear. Materials and Design, 206, 109808. doi:10.1016/j.matdes.2021.109808.

[8] Liu, K., Zong, S., Li, Y., Wang, Z., Hu, Z., & Wang, Z. (2022). Structural response of the U-type corrugated core sandwich panel used in ship structures under the lateral quasi-static compression load. Marine Structures, 84, 103198. doi:10.1016/j.marstruc.2022.103198.

[9] Zhu, F., & Lu, G. (2007). A review of blast and impact of metallic and sandwich structures. Electronic Journal of Structural Engineering, (1), 92-101.

[10] Cerik, B. C. (2017). Damage assessment of marine grade aluminium alloy-plated structures due to air blast and explosive loads. Thin-Walled Structures, 110, 123–132. doi:10.1016/j.tws.2016.10.021.

[11] Li, Y., Ren, X., Zhang, X., Chen, Y., Zhao, T., & Fang, D. (2021). Deformation and failure modes of aluminum foam-cored sandwich plates under air-blast loading. Composite Structures, 258, 113317. doi:10.1016/j.compstruct.2020.113317.

[12] Deqiang, S., Weihong, Z., & Yanbin, W. (2010). Mean out-of-plane dynamic plateau stresses of hexagonal honeycomb cores under impact loadings. Composite Structures, 92(11), 2609–2621. doi:10.1016/j.compstruct.2010.03.016.

[13] Nayak, S. K., Singh, A. K., Belegundu, A. D., & Yen, C. F. (2013). Process for design optimization of honeycomb core sandwich panels for blast load mitigation. Structural and Multidisciplinary Optimization, 47(5), 749–763. doi:10.1007/s00158-012-0845-x.

[14] Lee, J., Lacy, T. E., & Pittman, C. U. (2021). Lightning mechanical damage prediction in carbon/epoxy laminates using equivalent air blast overpressure. Composites Part B: Engineering, 212, 108649. doi:10.1016/j.compositesb.2021.108649.

[15] Karlos, V., & Solomos, G. (2013). Calculation of blast loads for application to structural components. JRC Technical reports, European Laboratory for Structural Assessment. Publications Office of the European Union, Luxemborg city, Luxemborg. doi:10.2788/61866.

[16] Fleck, N. A., & Deshpande, V. S. (2004). The resistance of clamped sandwich beams to shock loading. Journal of Applied Mechanics, Transactions ASME, 71(3), 386–401. doi:10.1115/1.1629109.

[17] Takeda, N., Minakuchi, S., & Okabe, Y. (2007). Smart Composite Sandwich Structures for Future Aerospace Application - Damage Detection and Suppression-: a Review. Journal of Solid Mechanics and Materials Engineering, 1(1), 3–17. doi:10.1299/jmmp.1.3.

[18] Sahoo, D. K., Guha, A., Tewari, A., & Singh, R. K. (2017). Performance of Monolithic Plate and Layered Plates under Blast Load. Procedia Engineering, 173, 1909–1917. doi:10.1016/j.proeng.2016.12.251.

[19] Liu, K., Zong, S., Li, Y., Wang, Z., Hu, Z., & Wang, Z. (2022). Structural response of the U-type corrugated core sandwich panel used in ship structures under the lateral quasi-static compression load. Marine Structures, 84, 103198. doi:10.1016/j.marstruc.2022.103198.

[20] Markose, A., & Rao, C. L. (2017). Mechanical response of V shaped plates under blast loading. Thin-Walled Structures, 115, 12–20. doi:10.1016/j.tws.2017.02.002.

[21] Wowk, D., Reyno, T., Yeung, R., & Marsden, C. (2020). An experimental and numerical investigation of core damage size in honeycomb sandwich panels subject to low-velocity impact. Composite Structures, 254, 112739. doi:10.1016/j.compstruct.2020.112739.

[22] Zhao, C., He, K., Zhi, L., Lu, X., Pan, R., Gautam, A., Wang, J., & Li, X. (2021). Blast behavior of steel-concrete-steel sandwich panel: Experiment and numerical simulation. Engineering Structures, 246, 112998. doi:10.1016/j.engstruct.2021.112998.

[23] Jing, L., Liu, K., Su, X., & Guo, X. (2021). Experimental and numerical study of square sandwich panels with layered-gradient foam cores to air-blast loading. Thin-Walled Structures, 161, 107445. doi:10.1016/j.tws.2021.107445.

[24] Mary Varghese, R., & Mary Varghese, K. (2022). Comparative study on the blast load response of woven and lattice core metallic sandwich panels. Materials Today: Proceedings. doi:10.1016/j.matpr.2022.04.257.

[25] Zhang, C., Tan, P. J., & Yuan, Y. (2022). Confined blast loading of steel plates with and without pre-formed holes. International Journal of Impact Engineering, 163, 104183. doi:10.1016/j.ijimpeng.2022.104183.

[26] Shrot, A., & Bäker, M. (2012). Determination of Johnson-Cook parameters from machining simulations. Computational Materials Science, 52(1), 298–304. doi:10.1016/j.commatsci.2011.07.035.

[27] Nemat-Nasser, S., Guo, W. G., & Kihl, D. P. (2001). Thermomechanical response of AL6XN stainless steel over a wide range of strain rates and temperatures. Journal of the Mechanics and Physics of Solids, 49(8), 1823–1846. doi:10.1016/S0022-5096(00)00069-7.

[28] Abed, F. H., & Voyiadjis, G. Z. (2005). Plastic deformation modeling of AL-6XN stainless steel at low and high strain rates and temperatures using a combination of bcc and fcc mechanisms of metals. International Journal of Plasticity, 21(8), 1618–1639. doi:10.1016/j.ijplas.2004.11.003.

[29] Prabowo, A. R., Tuswan, T., Nurcholis, A., & Pratama, A. A. (2021). Structural Resistance of Simplified Side Hull Models Accounting for Stiffener Design and Loading Type. Mathematical Problems in Engineering, 2021, 1–19. doi:10.1155/2021/6229498.

[30] Akbar, M. S., Prabowo, A. R., Tjahjana, D. D. D. P., & Tuswan, T. (2021). Analysis of plated-hull structure strength against hydrostatic and hydrodynamic loads: A case study of 600 TEU container ships. Journal of the Mechanical Behavior of Materials, 30(1), 237–248. doi:10.1515/jmbm-2021-0025.

[31] Fajri, A., Prabowo, A. R., & Muhayat, N. (2022). Assessment of ship structure under fatigue loading: FE benchmarking and extended performance analysis. Curved and Layered Structures, 9(1), 163–186. doi:10.1515/cls-2022-0014.

[32] Prabowo, A. R., Baek, S. J., Cho, H. J., Byeon, J. H., Bae, D. M., & Sohn, J. M. (2017). The effectiveness of thin-walled hull structures against collision impact. Latin American Journal of Solids and Structures, 14(7), 1345–1360. doi:10.1590/1679-78253895.

[33] Prabowo, A. R., Cao, B., Sohn, J. M., & Bae, D. M. (2020). Crashworthiness assessment of thin-walled double bottom tanker: Influences of seabed to structural damage and damage-energy formulae for grounding damage calculations. Journal of Ocean Engineering and Science, 5(4), 387–400. doi:10.1016/j.joes.2020.03.002.

[34] Prabowo, A. R., Ridwan, R., & Muttaqie, T. (2022). On the Resistance to Buckling Loads of Idealized Hull Structures: FE Analysis on Designed-Stiffened Plates. Designs, 6(3), 46. doi:10.3390/designs6030046.

[35] Gagnon, R. E., & Wang, J. (2012). Numerical simulations of a tanker collision with a bergy bit incorporating hydrodynamics, a validated ice model and damage to the vessel. Cold Regions Science and Technology, 81, 26–35. doi:10.1016/j.coldregions.2012.04.006.

[36] Alabdullah, M., Polishetty, A., Nomani, J., & Littelfair, G. (2016). Experimental and finite element analysis of machinability of AL6XN super austenitic stainless steel. The International Journal of Advanced Manufacturing Technology, 91(1-4), 501–516. doi:10.1007/s00170-016-9766-y.